NRQCD analysis of pion-induced charmonium production in fixed-target experiments
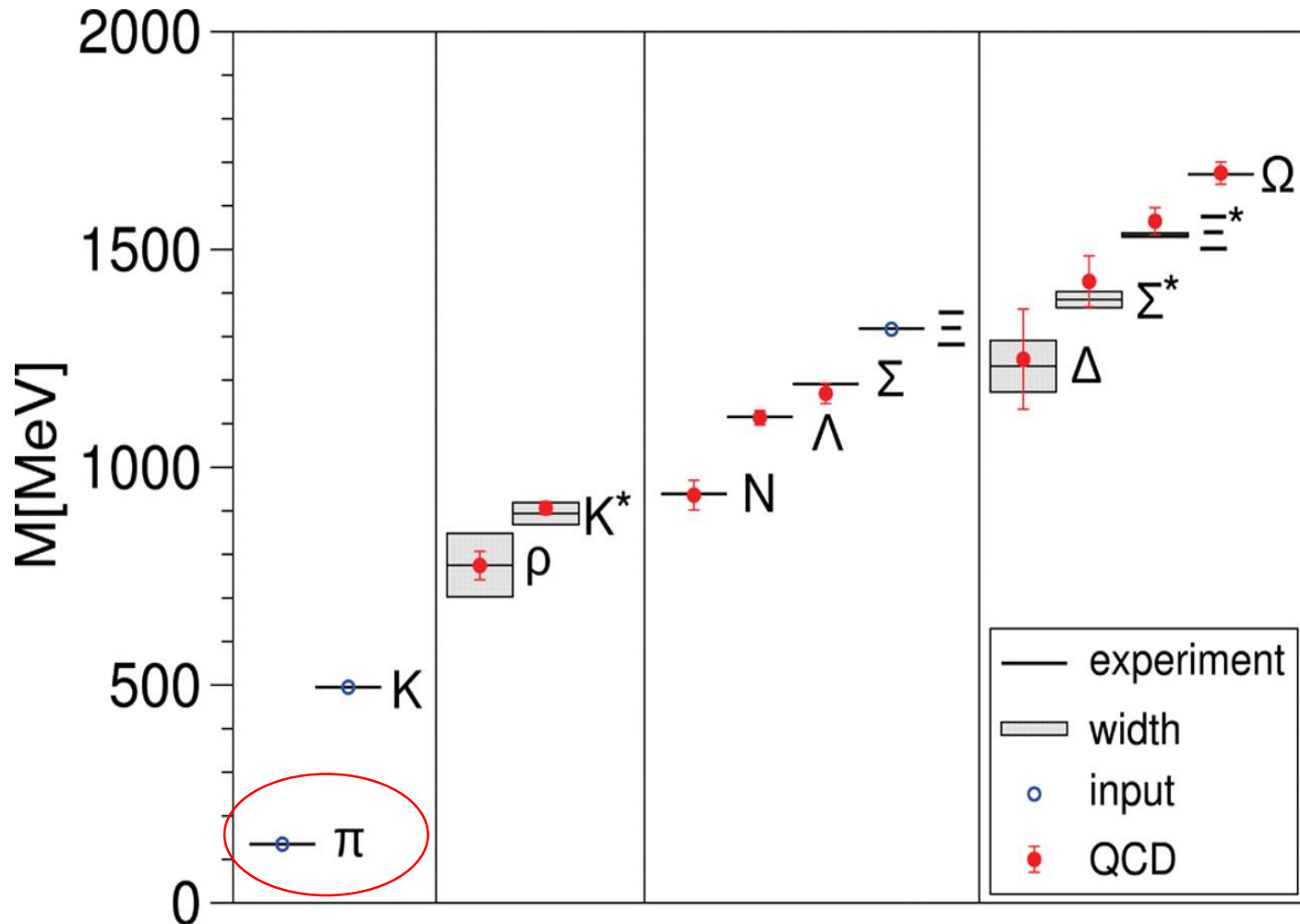
Wen-Chen Chang

Institute of Physics, Academia Sinica, Taiwan

In collaboration with
Chia-Yu Hsieh, Yu-Shiang Lian, Jen-Chieh Peng,
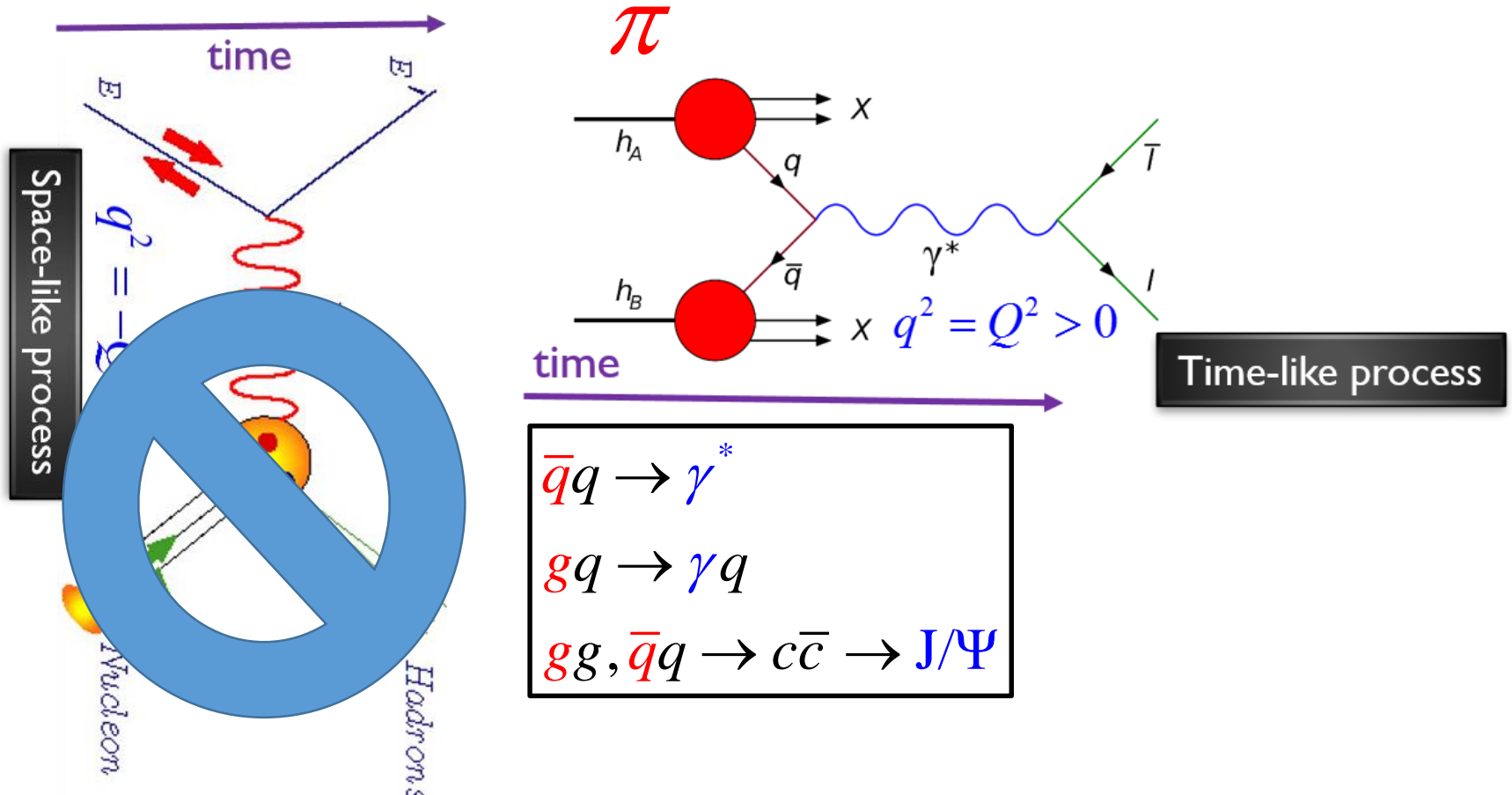Stephane Platchkov and Takahiro Sawada

Light hadron spectrum

Experimental Approach for Pion PDFs

$\overline{q}q \rightarrow \gamma^{*}$

$gq \rightarrow \gamma q$

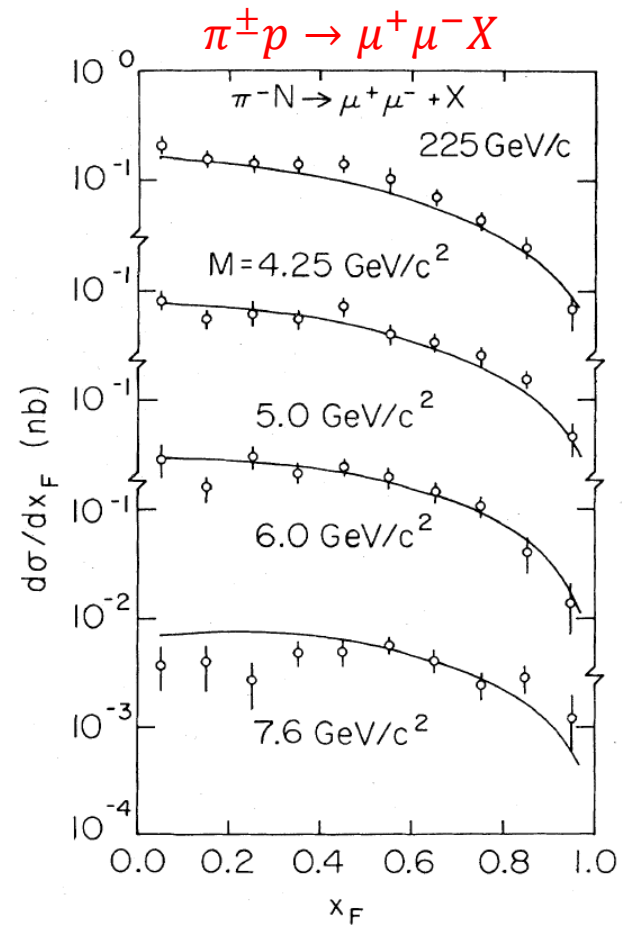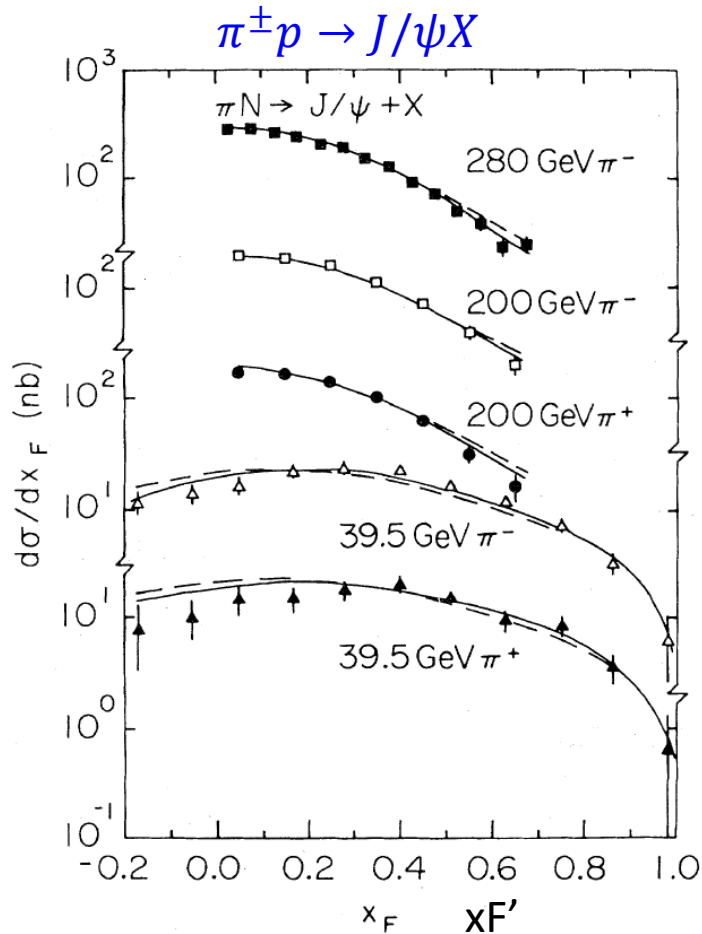$gg, \overline{q}q \rightarrow c\overline{c} \rightarrow J/\Psi$

No rest targets of pions!

3

Pion-induced Reactions

- Drell-Yan: $\pi^{\pm}p \rightarrow \mu^+\mu^- X$ (sensitive to valence quarks)
  - **LO:** $\boldsymbol{q\bar{q} \rightarrow \mu^+\mu^-}$
  - NLO: $q\bar{q} \rightarrow \mu^+\mu^- G, qG \rightarrow \mu^+\mu^- q$
  - NNLO: $q\bar{q}G \rightarrow \mu^+\mu^- G, qG \rightarrow \mu^+\mu^- qG, GG \rightarrow \mu^+\mu^- q\bar{q}$
- Direct photon: $\pi^{\pm}p \rightarrow \gamma X$ (sensitive to gluons)
  - **LO:** $\boldsymbol{q\bar{q} \rightarrow \gamma G, qG \rightarrow \gamma q}$
- Jpsi: $\pi^{\pm}p \rightarrow J/\psi X$ (sensitive to gluons)
  - **LO:** $\boldsymbol{q\bar{q} \rightarrow c\bar{c} \rightarrow J/\psi X, GG \rightarrow c\bar{c} \rightarrow J/\psi X}$
  - NLO: $q\bar{q} \rightarrow c\bar{c}G \rightarrow J/\psi X, GG \rightarrow c\bar{c}G \rightarrow J/\psi X, qG \rightarrow c\bar{c}q \rightarrow J/\psi X$
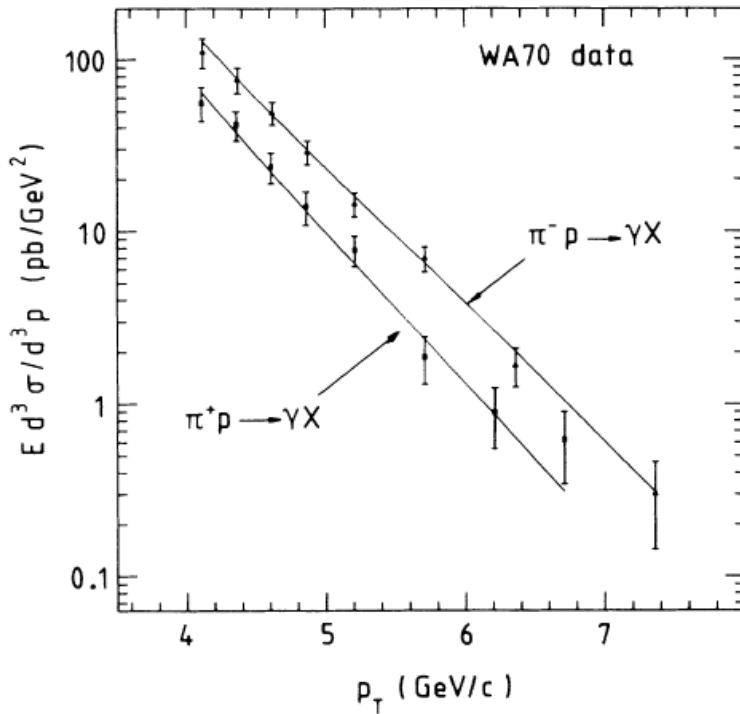
OW pion PDF
[J.F. Owens, PRD 30, 943 (1984)]

$\pi^{\pm}p \to J/\psi X$

$\pi^{\pm}p \to \mu^{+}\mu^{-}X$
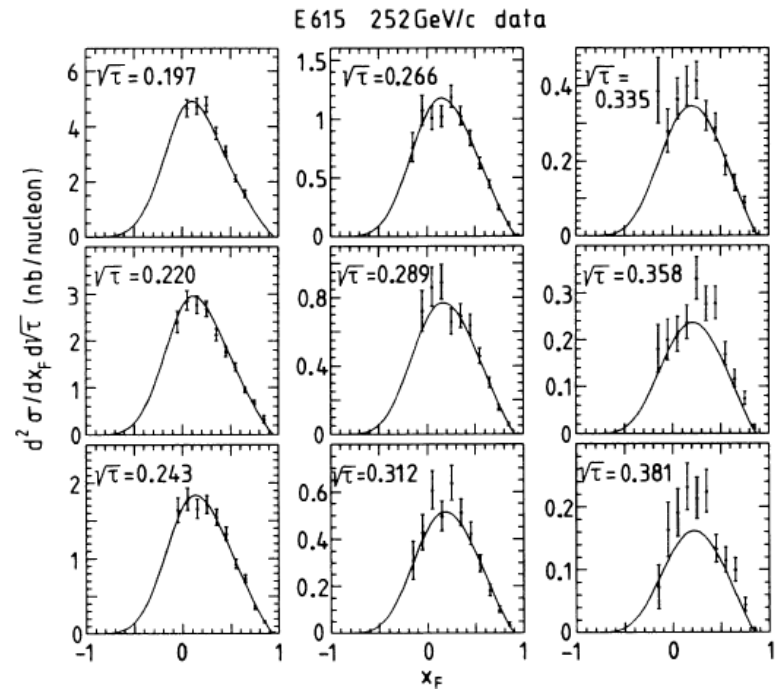

Fits to data of J/psi and DY production.

SMRS
[Sutton et al., PRD 45, 2349 (1992)]

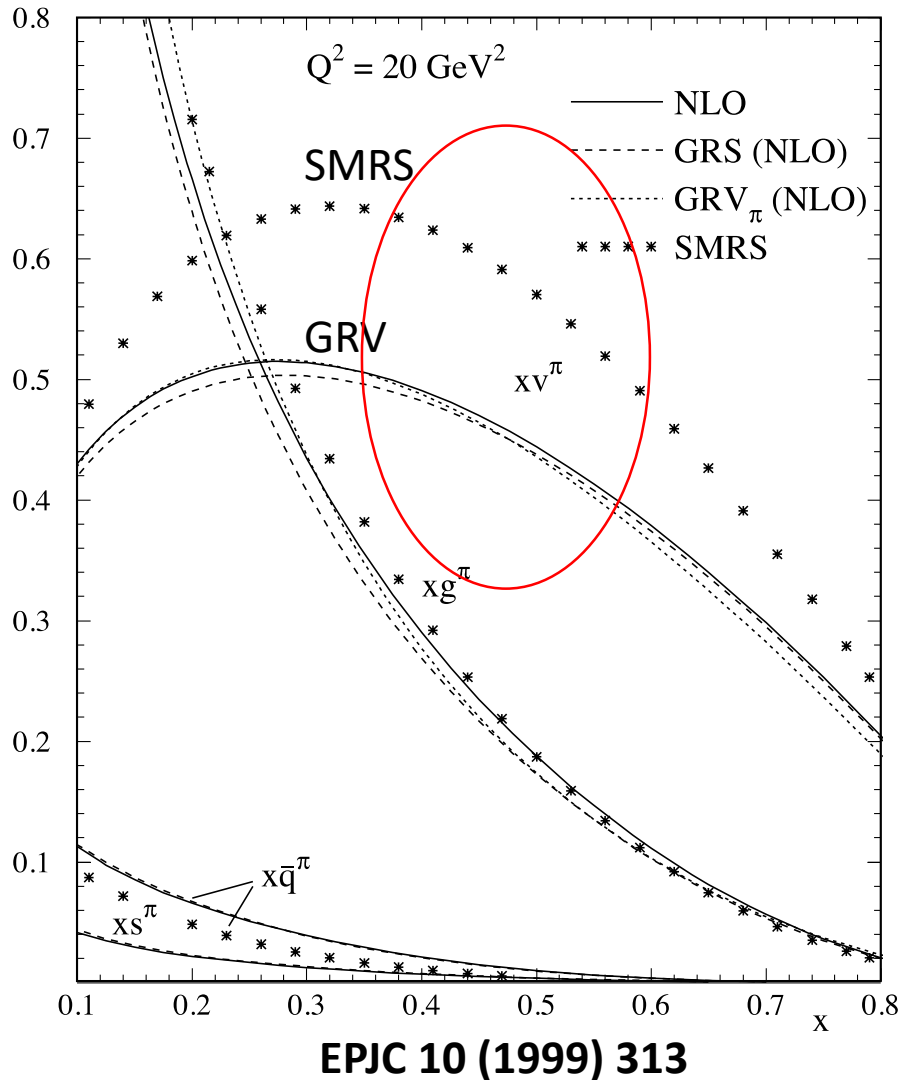$$\pi^{\pm} p \to \gamma X$$

$$\pi^{\pm} p \to \mu^{+}\mu^{-} X$$

Fits to data of direct-γ and DY production.

Pion PDFs (before 2018)

| PDF	DY	Direct γ	J/ψ	LN	Refs.
OW	*		*		[PRD 1984](#)
ABFKW	*	*			[PLB 1989](#)
SMRS	*	*			[PRD 1992](#)
GRV	*	*			[ZPC 1992](#)
GRS	*				[EPJC 1999](#)

- **Valence quarks** are well constrained by Drell-Yan data.
- **Sea and gluons** are constrained by the number of valence quarks and the momentum sum rule.
- Direct photon and J/psi data help to better constrain the gluons and thus sea quarks.
- GRS: relating sea quarks and gluons by a constituent quark model.

Pion PDFs (before 2018)

$Q^2 = 20 \text{ GeV}^2$

SMRS

GRV

xv^π

xg^π

$x\bar{q}^\pi$

xs^π

|	NLO
	GRS (NLO)
	GRV_π (NLO)
	SMRS

EPJC 10 (1999) 313

- PDFs were mainly determined by Drell-Yan, single γ, J/psi data.
- **20% difference of valence quarks at x = 0.5 !**

JAM18: Include leading neutron (LN) electroproduction from HERA
[Barry et al., PRL 121, 152001 (2018)]
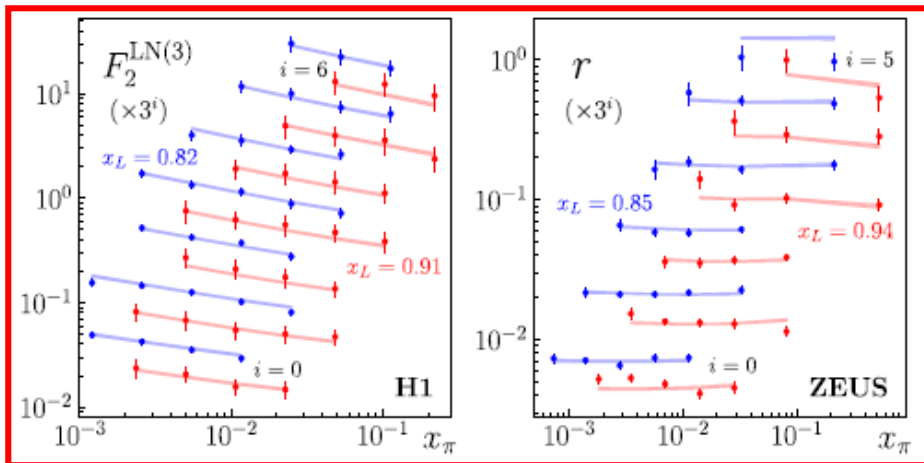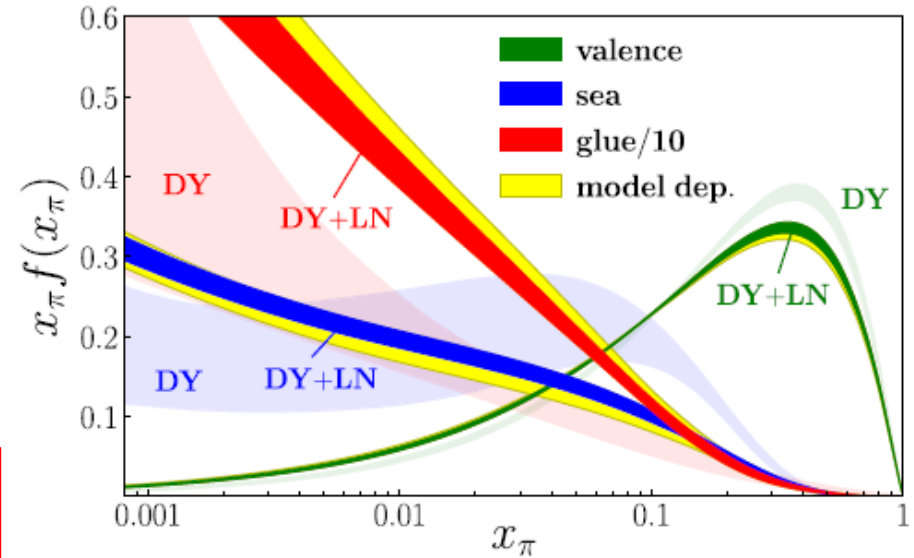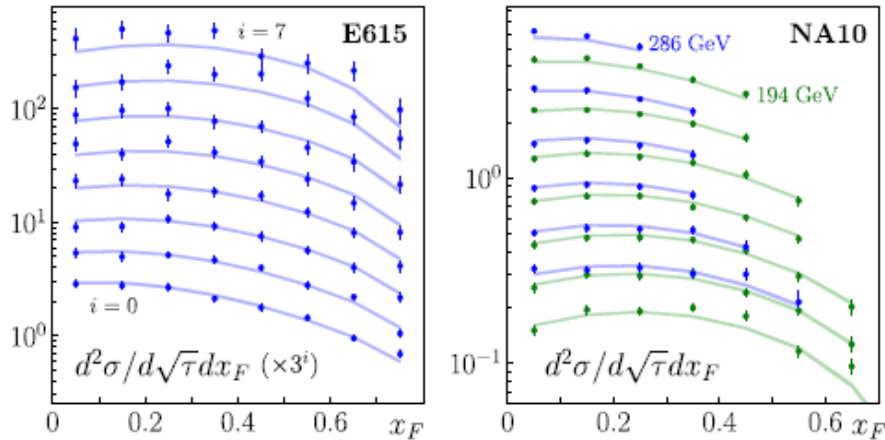
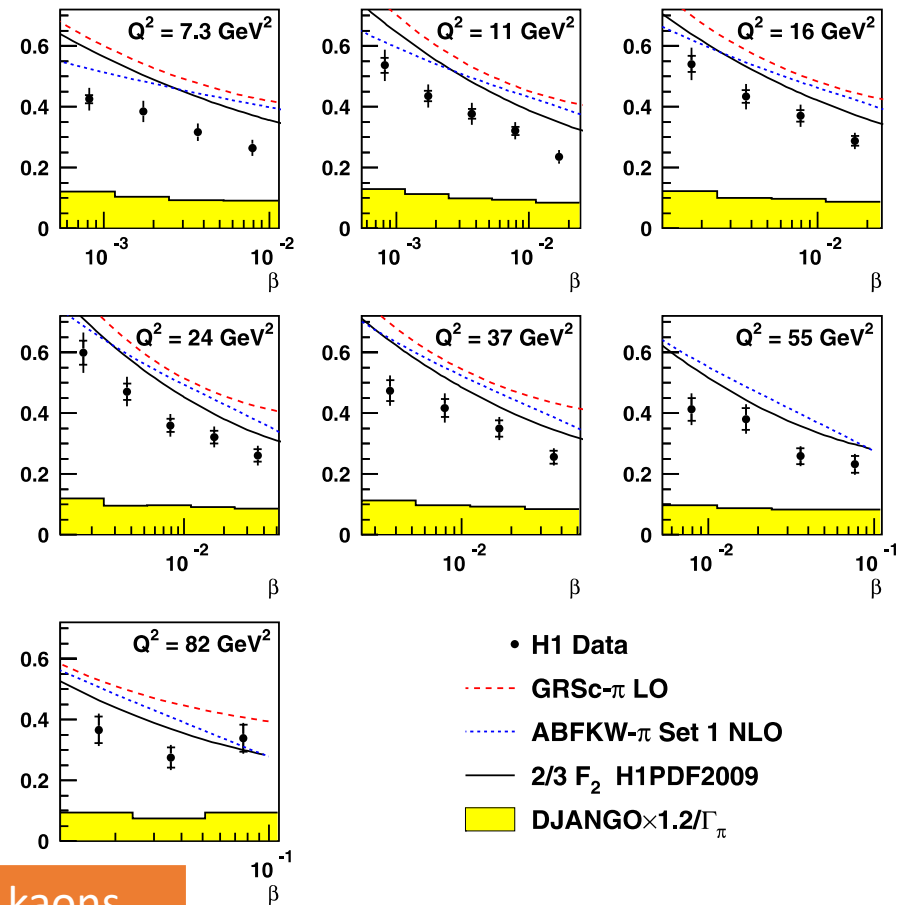- Uncertainties are much reduced using DY+LN, as compared to DY alone.

Leading neutron (LN) electroproduction from HERA

Experimentally tagged
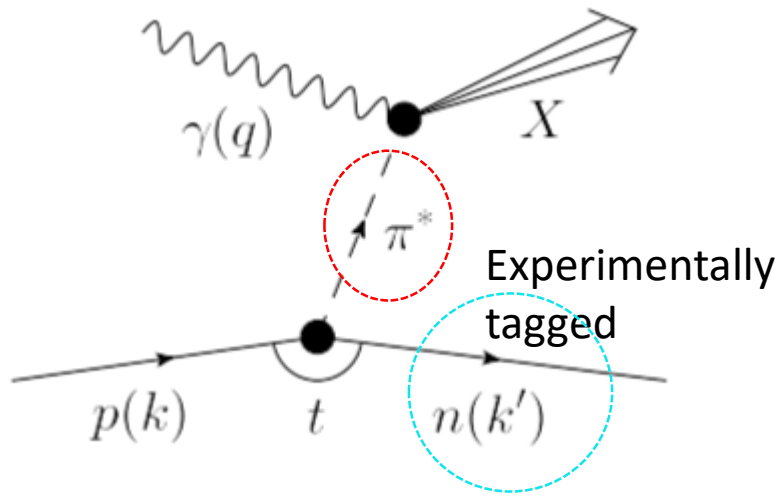
Sullivan processes from a nucleon's pion cloud

$F_2^{LN(3)}(x_L = 0.73)/\Gamma_\pi$, $\Gamma_\pi = 0.13$　　　H1

$Q^2 = 7.3$ GeV^2
$Q^2 = 11$ GeV^2
$Q^2 = 16$ GeV^2
$Q^2 = 24$ GeV^2
$Q^2 = 37$ GeV^2
$Q^2 = 55$ GeV^2
$Q^2 = 82$ GeV^2

- H1 Data
- GRSc-π LO
- ABFKW-π Set 1 NLO
- 2/3 F_2 H1PDF2009
- DJANGO$\times$1.2/Γ_π

Off-shell persistence of composite pions and kaons
S.X. Qin et al., PRC 97, 015203 (2018)
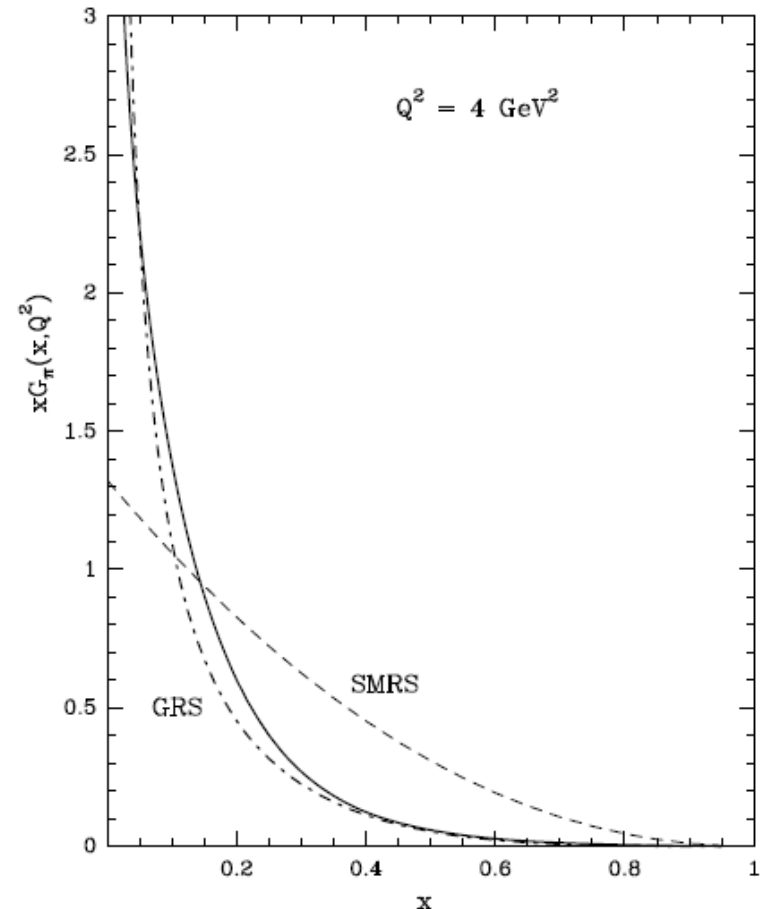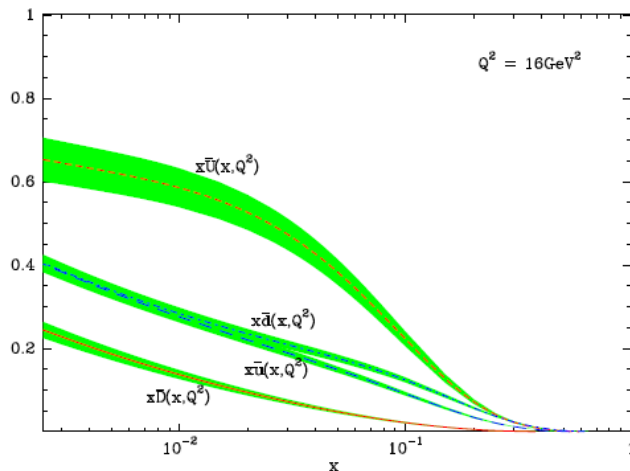
10

Statistical approach
[Bourrely and Soffer, NPA 981, 118 (2019)]

$$xQ^{\pm}(x) = \frac{A_Q X_Q^{\pm} x^{b_Q}}{\exp[(x - X_Q^{\pm})/\bar{x}] + 1}$$

$$x\bar{Q}^{\pm}(x) = \frac{\bar{A}(X_Q^{\mp})^{-1} x^{\bar{b}}}{\exp[(x + X_Q^{\mp})/\bar{x}] + 1}$$

$$xG_{\pi}(x) = A_G x^{b_G} / (\exp(x/\bar{x}) - 1)$$

$\bar{x}$=0.09: a universal temperature

xFitter:
[Novikov et al., PRD 102, 014040 (2020), arXiv:2002.02902]

Experiment	Normalization uncertainty	Normalization factor	χ^2/N_{points}
E615	15 %	1.160 ± 0.020	206/140
NA10 (194 GeV)	6.4%	0.997 ± 0.014	107/67
NA10 (286 GeV)	6.4%	0.927 ± 0.013	95/73
WA70	32%	0.737 ± 0.012	64/99

Figure 3 shows the obtained pion PDFs in comparison to a recent analysis by JAM [26], and to GRVPI1 [22] — the only set available in the LHAPDF6 [39] library. The new valence distribution presented here is in good agreement with JAM, and both disagree with the early GRV analysis. The relatively difficult to determine sea and gluon distributions are different in all three PDF sets, however, this new PDF and the JAM determination agree within the larger uncertainties of our fit.
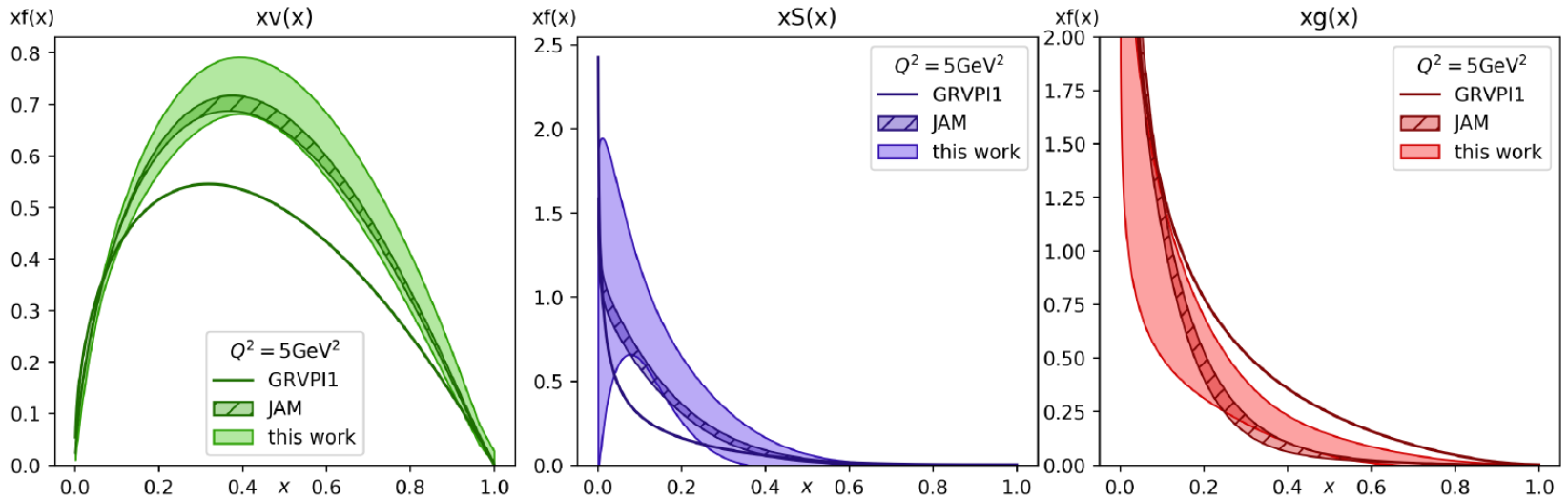

FIG. 3. Comparison between the pion PDFs obtained in this work, a recent determination by the JAM collaboration [26], and the GRVPI1 pion PDF set [22].
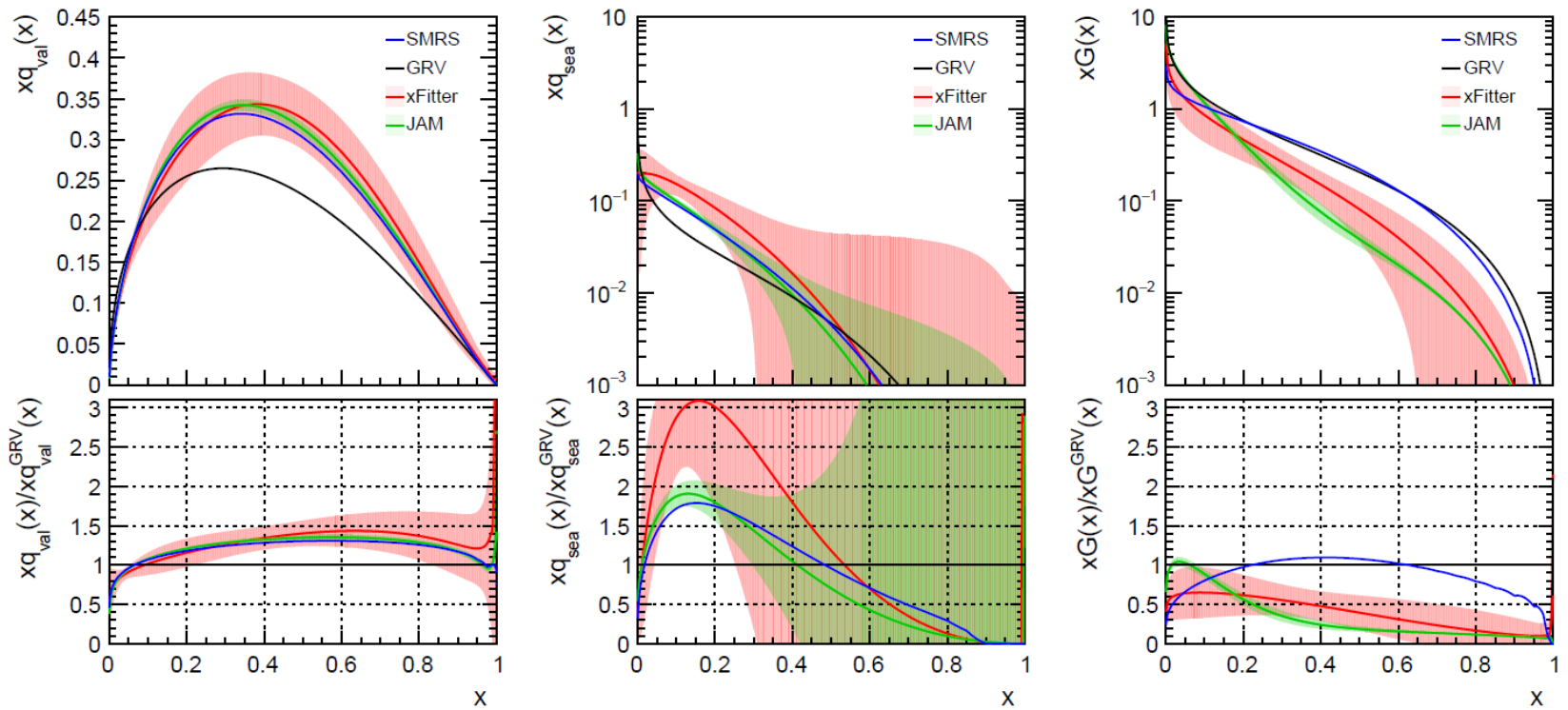
xFitter is consistent with JAM but disagrees with GRV.

Pion PDFs (2020)

PDF	DY	Direct γ	J/ψ	LN	Refs.
OW	*		*		PRD 1984
ABFKW	*	*			PLB 1989
SMRS	*	*			PRD 1992
GRV	*	*			ZPC 1992
GRS	*				EPJC 1999
JAM	*			*	PRL 2018
BS	*				NPA 2019 PLB 2021
xFitter	*	*			PRD 2020

Pion PDFs

$$Q^2 = 9.6 \text{ GeV}^2$$

Pion PDFs from Theoretical Models

- **Chiral-quark model** (Nam 2012, Watanabe 2016, Watanabe 2017)

- **Nambu-Jona-Lasinio model** (Hutauruk 2016)

- **Light-front Hamiltonian** (Lan 2019)

- **Holographic QCD** (deTeramond 2018, Watanabe 2019, Lan 2020)

- **Maximum entropy method** (Han 2018, 2020)

- **Dyson-Schwinger equations** (Chang 2014, Chang 2014, Chen 2016, Shi 2018, Bednar 2018, Ding 2019, Cui 2020)

Pion PDFs from Lattice QCD
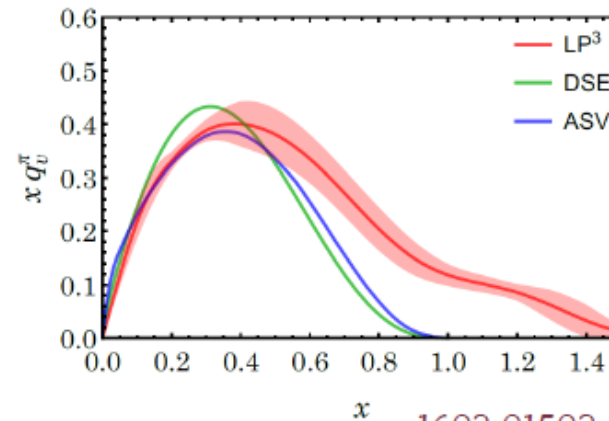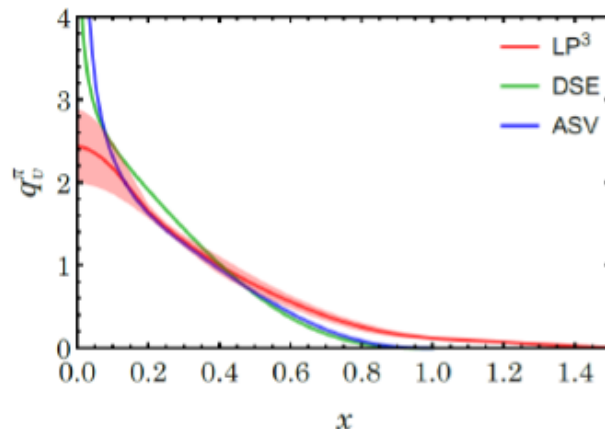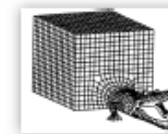## Z.H. Zhang et al., PRD 100, 034505 (2019)

Pion PDF

§ Not trivial to calculate in reality either

§ The first lattice exploratory study

1804.01483 (LP³)

$\gg M_\pi \approx 310$ MeV, $a \approx 0.12$ fm ($M_\pi L \approx 4.5$)

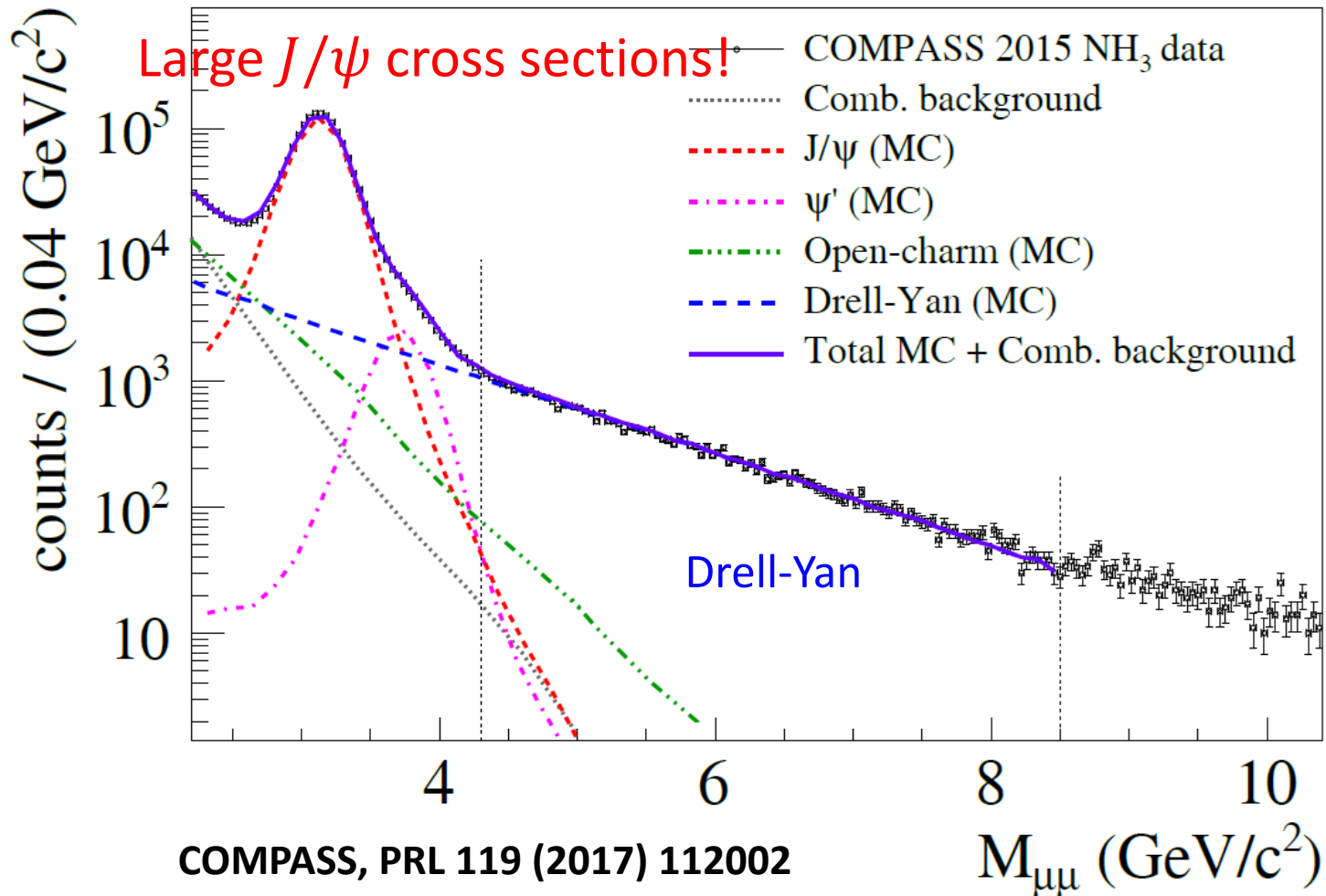§ Study of systematics needed

$\gg$ Lattice-spacing, finite-volume, larger P_z, ...

1602.01502 (DSE)
1009.2481 (ASV)

H.W. Lin, JLAB pieic2018 workshop

16

Dimuon Invariant-mass Spectrum
(COMPASS Pion-Induced 2015 Drell-Yan Run)

Large J/ψ cross sections!

COMPASS 2015 NH$_3$ data
Comb. background
J/ψ (MC)
ψ' (MC)
Open-charm (MC)
Drell-Yan (MC)
Total MC + Comb. background

Drell-Yan

COMPASS, PRL 119 (2017) 112002

Pion-induced J/psi Production - Fixed-target Experiments

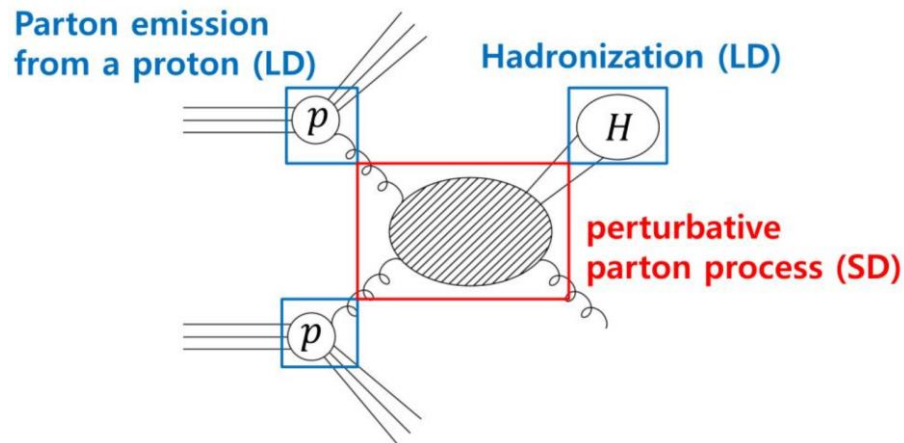| Paper	Reference	Year	Collab	E (GeV)	sqrt(s) (GeV)	Beam	Targets
Fermilab							
Branson	PRL 23, 1331	1977	Princ-Chicago	225	20.5	$\pi-$, $\pi+$, p	C, Sn
Anderson	PRL 42, 944	1979	E444	225	20.5	$\pi-$, $\pi+$, K+, p, ap	C, Cu, W
Abramov	Fermi 91-062-E	1991	E672/E706	530	31.5	$\pi-$	Be
Kartik	PRD 41, 1	1990	E672	530	31.5	$\pi-$	C, AL, Cu, Pb
Katsanevas	PRL 60, 2121	1988	E537	125	15.3	$\pi-$, ap	Be, Cu, W
Akerlof	PR D48, 5067	1993	E537	125	15.3	$\pi-$, ap	Be, Cu, W
Antoniazzi	PRD 46, 4828	1992	E705	300	23.7	$\pi-$, $\pi+$	Li
Gribushin	PR D53, 4723	1995	E672/E706	515	31.1	$\pi-$	Be
Koreshev	PRL 77, 4294	1996	E706/E672	515	31.1	$\pi-$	Be
CERN							
Abolins	PLB 82, 145	1979	WA11/Goliath	150	16.8	$\pi-$	Be
McEwen	PLB 121, 198	1983	WA11	190	18.9	$\pi-$	Be
Badier	Z.Phys. C20, 101	1983	NA3	150	16.8	$\pi-$, $\pi+$, K-, K+, p, ap	H, Pt
"	"	1983	NA3	200	19.4	$\pi-$, $\pi+$, K-, K+, p, ap	H, Pt
"	"	1983	NA3	280	22.9	$\pi-$, $\pi+$, K-, K+, p, ap	H, Pt
Corden	PLB 68, 96	1977	WA39	39.5	8.6	$\pi-$, $\pi+$, K-, K+, p, ap	Cu
Corden	PLB 96, 411	1980	WA39	39.5	8.6	$\pi-$, $\pi+$, K-, K+, p, ap	W
Corden	PLB 98, 220	1981	WA39	39.5	8.6	$\pi-$, $\pi+$, K-, K+, p, ap	p
Corden	PLB 110, 415	1982	WA40	39.5	8.6	$\pi-$, $\pi+$, K-, K+, p, ap	p, W
Alexandrov	NPB 557, 3	1999	Beatrice	350	25.6	$\pi-$	Si, C, W

Goals of Our Studies

- **Pion PDFs**: SMRS, GRV, xFitter and JAM with different gluon strength at large-x.

- Gluon fusion process is the LO Jpsi production mechanism.

- **Can we differentiate them by the pion-induced $\sigma(\sqrt{s}, x_F)$ of Jpsi production over a wide range of beam energy – [40, 515] GeV?**

$$Q^2 = 9.6 \text{ GeV}^2$$
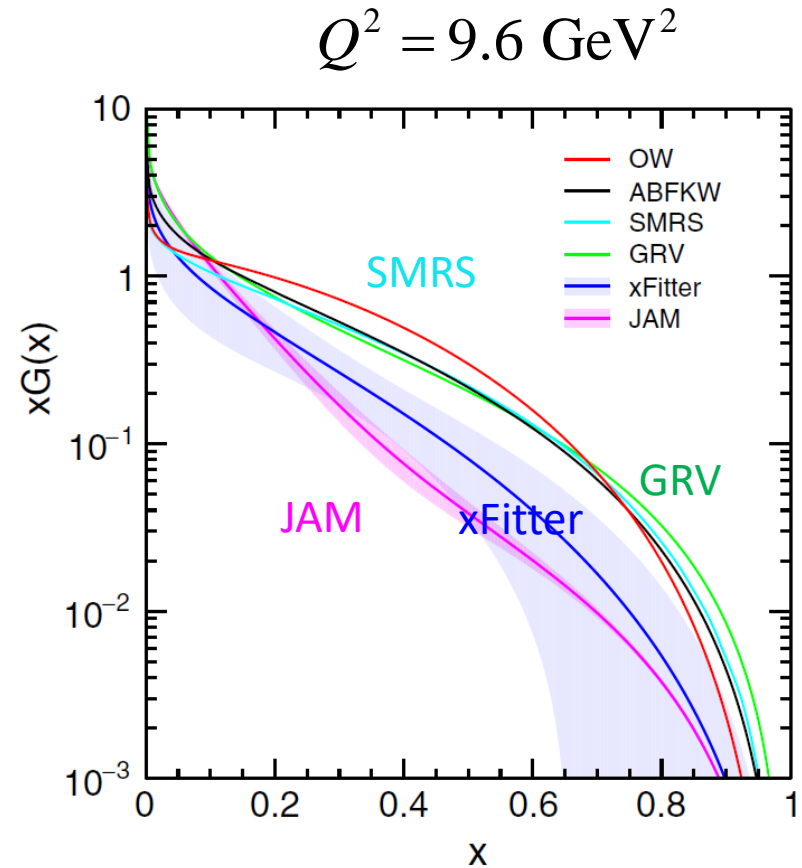
Model Dependence of $c\bar{c}$ pair Hadronizing

- **Color singlet model (CSM)**: only pairs with matched quantum number of the charmonium.

- **Color evaporation model (CEM)**: all pairs with mass less than $D\bar{D}$ threshold. One hadronization parameter for each charmonium.

- **Non-relativistic QCD model (NRQCD)**: all pairs of different color and spin sates fragmenting with different probabilities – long-distance matrix elements (LDMEs).

Parton emission from a proton (LD)

Hadronization (LD)

perturbative parton process (SD)

Color evaporation model (CEM)

Constraining gluon density of pions at large x by pion-induced J/ψ production

Wen-Chen Chang

Institute of Physics, Academia Sinica, Taipei 11529, Taiwan

Jen-Chieh Peng

Department of Physics, University of Illinois at Urbana-Champaign, Urbana, Illinois 61801, USA

Stephane Platchkov

IRFU, CEA, Université Paris-Saclay, 91191 Gif-sur-Yvette, France

Takahiro Sawada

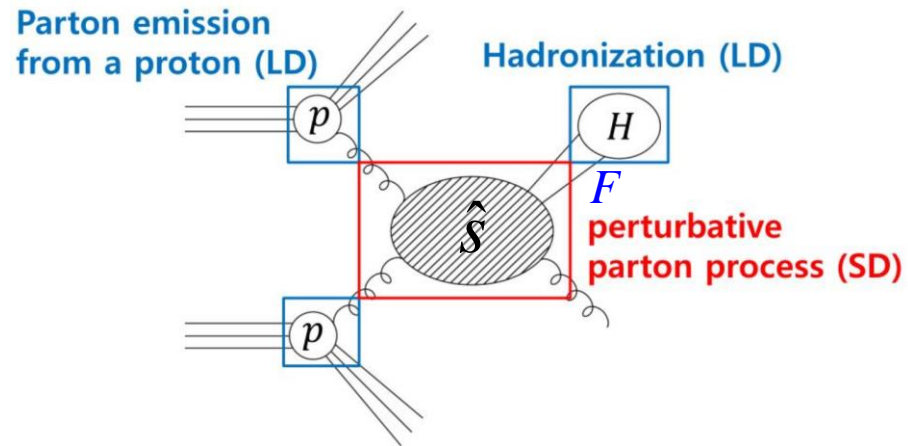*Department of Physics, Osaka City University, Osaka 558-8585, Japan*

The gluon distributions of the pion obtained from various global fits exhibit large variations among them. Within the framework of the color evaporation model, we show that the existing pion-induced J/ψ

Color Evaporation Model

$$\sigma[AB \rightarrow J/\psi X]$$

$$= F \sum_{i,j} \int_{2m_c}^{2m_D} d\hat{s} \int dx_1 dx_2 f_{i/A}(x_1, \mu_F) f_{j/B}(x_2, \mu_F)$$

$$\hat{\sigma}[ij \rightarrow c\overline{c}X](x_1 P_A, x_2 P_B, \mu_F, \mu_R)\delta(\hat{s} - x_1 x_2 s)$$

Parton emission from a proton (LD)

Hadronization (LD)

p H F

$\hat{s}$ **perturbative parton process (SD)**

p

LO/NLO calculations of $\hat{\sigma}[ij \rightarrow c\overline{c}X]$:

- P. Nason, S. Dawson and R.K. Ellis, Nucl. Phys. B303 (1988) 607
- M.L. Mangano, P. Nason and G. Ridolfi, Nucl. Phys. B405 (1993) 507

LO & NLO Diagrams

q$\bar{\text{q}}$

GG

qG

A. Petrelli et al./Nuclear Physics B 514 (1998) 245–309

D_0

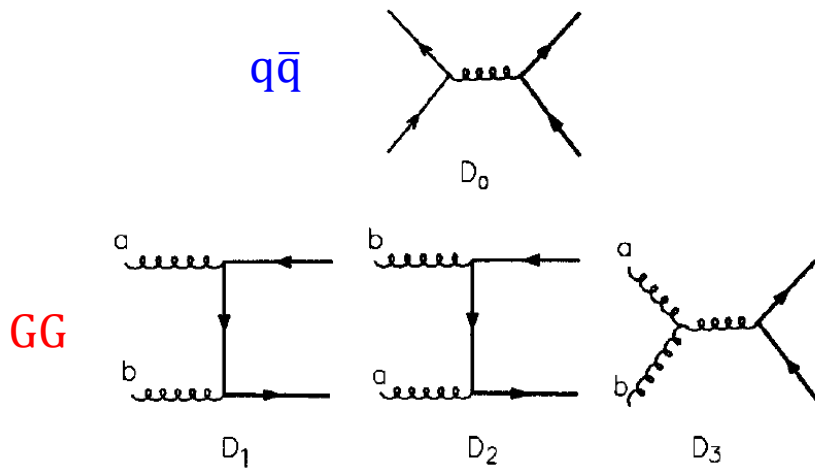D_1 D_2 D_3

Fig. 2. Diagrams for the $q\bar{q}$ and gg Born amplitudes.

A. Petrelli et al./Nuclear Physics B 514 (1998) 245–309   287
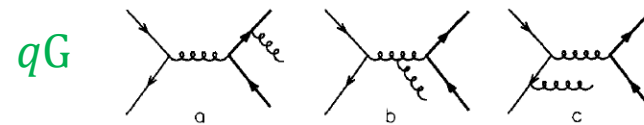
a   b   c

Fig. 8. Diagrams for the real corrections to the $q\bar{q}$ channels. Permutations of outgoing gluons and/or reversal of fermion lines are always implied.
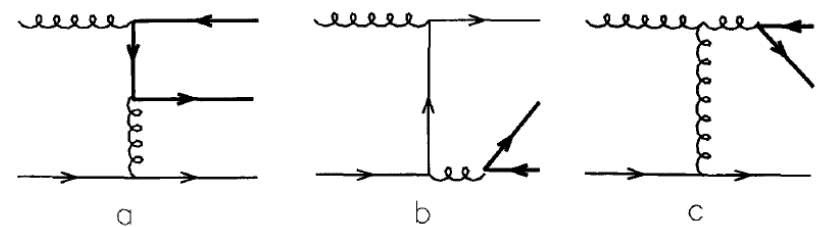
286   A. Petrelli et al./Nuclear Physics B 514 (1998) 245–309
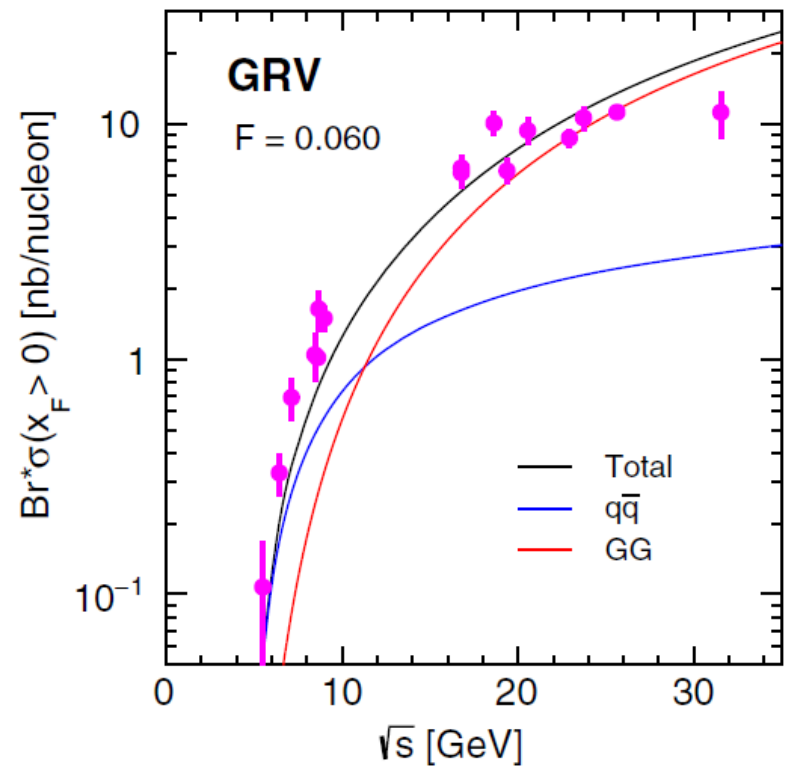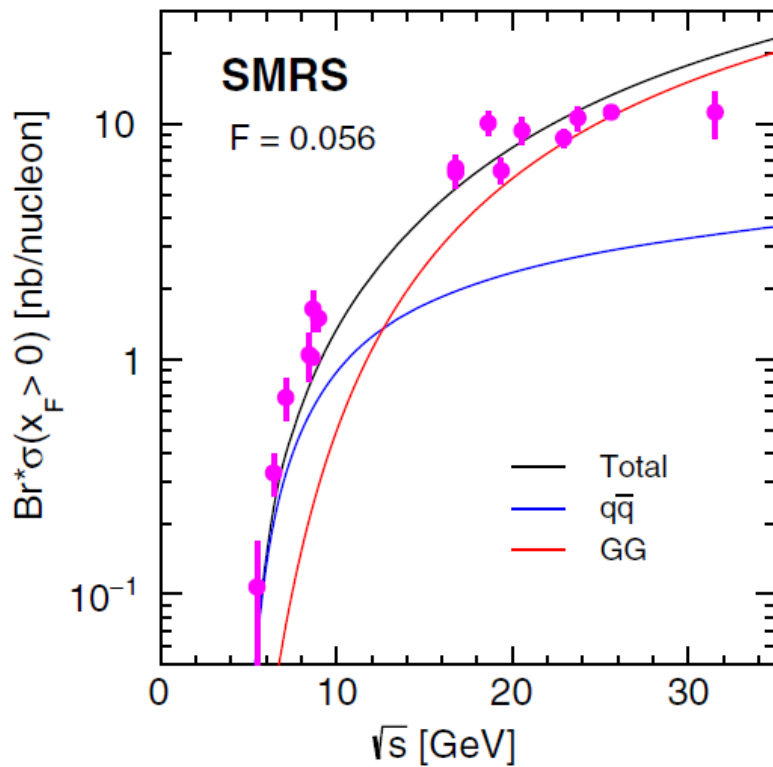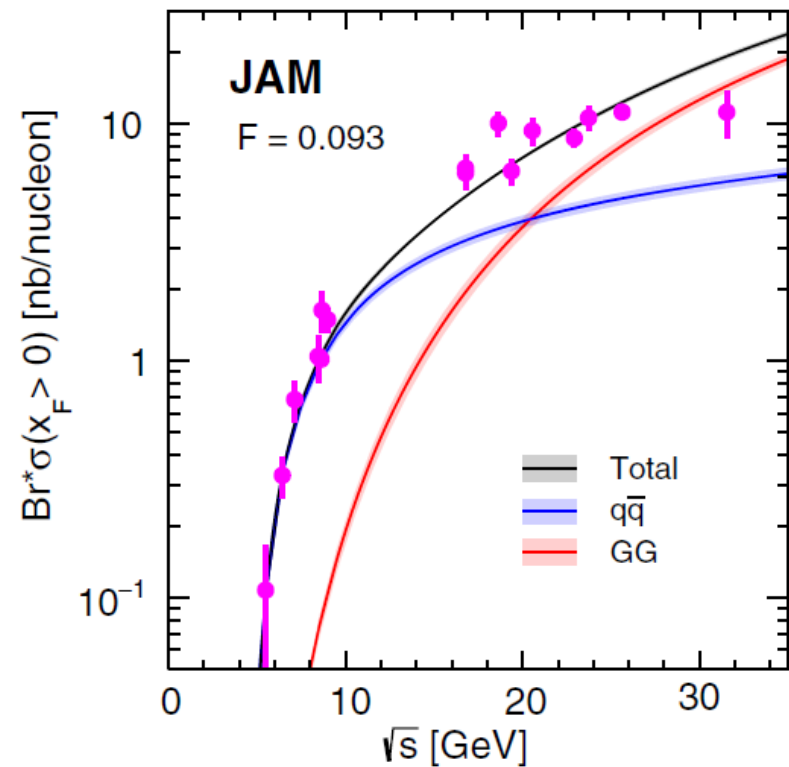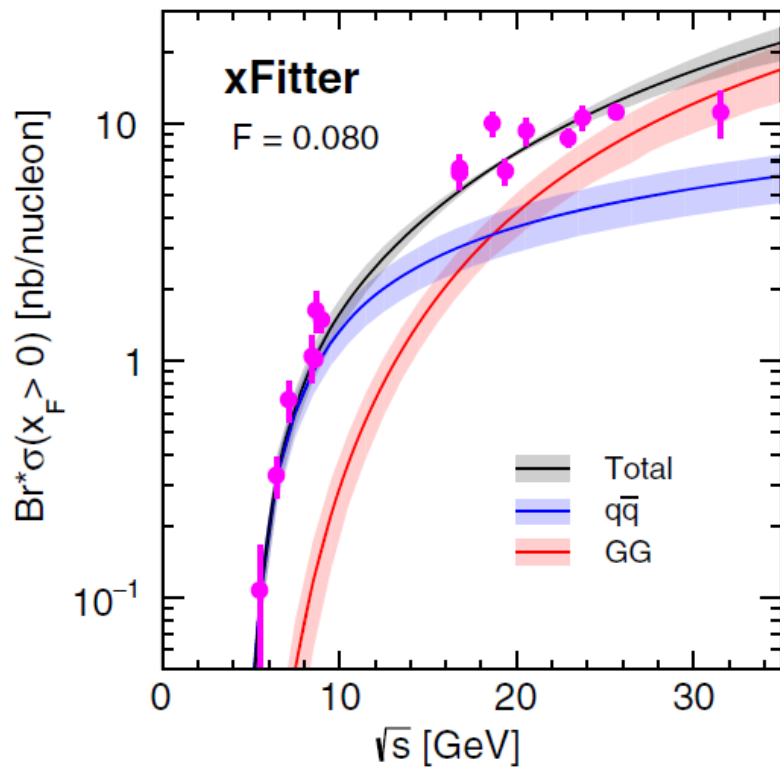
a   b   c

Fig. 7. Diagrams for the gq channels. Reversal of fermion lines is always implied.

23

Data vs. CEM NLO
: Energy dependence

GG dominates at high energies while qqbar is important near threshold.

Data vs. CEM NLO
: Energy dependence

GG dominates at high energies while qqbar is important near threshold.

Data of $d\sigma/dx_F$

TABLE II. The J/ψ production datasets with π^- beam used in the analysis, listed in order of decreasing beam momentum.
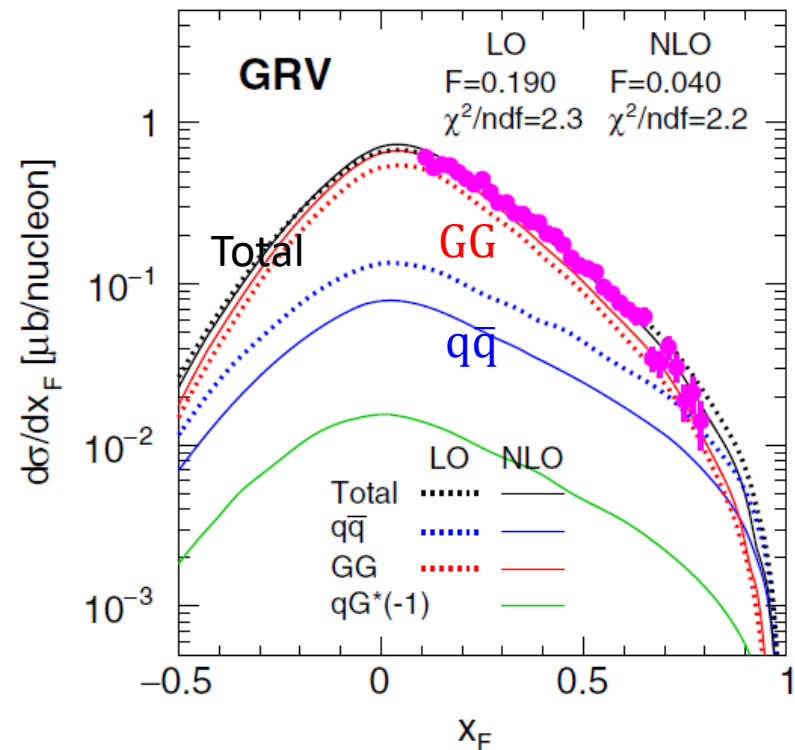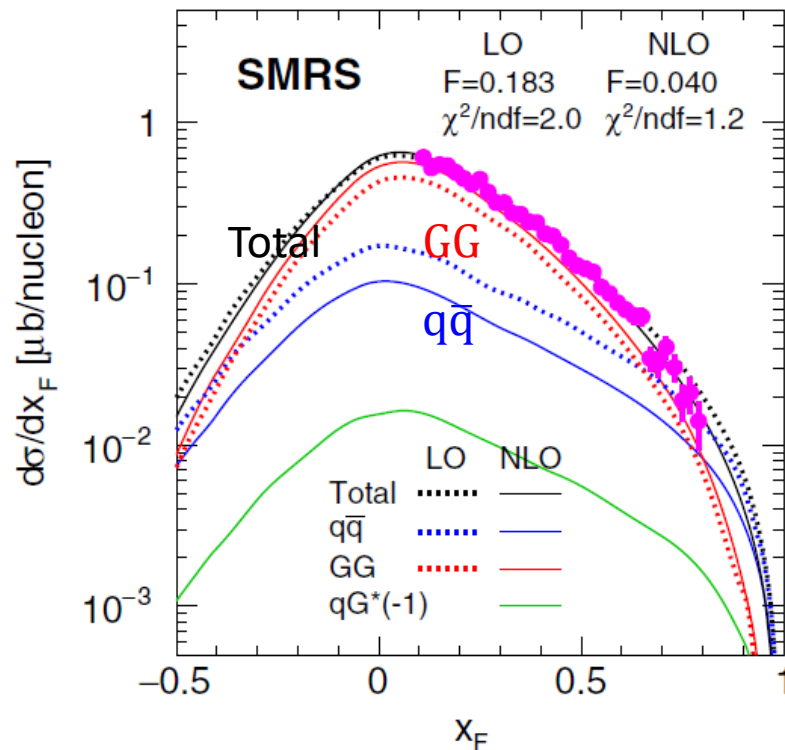
Experiment	P_{beam} (GeV/c)	Target	Normalization[a]	References
FNAL E672, E706	515	Be	12.0	[68]
FNAL E705	300	Li	9.5	[69]
CERN NA3[b]	280	p	13.0	[70]
CERN NA3[b]	200	p	13.0	[70]
CERN WA11[b]	190	Be	[c]	[72]
CERN NA3[b]	150	p	13.0	[70]
FNAL E537	125	Be	6.0	[73]
CERN WA39[b]	39.5	p	15.0	[74]

Data vs. CEM LO/NLO

$[\pi^- + Be \to Jpsi + X$ at **515 GeV**, PRD 53, 4723 (1996)]

m_c=1.5 GeV, μ_F=2m_c, μ_R=m_c,
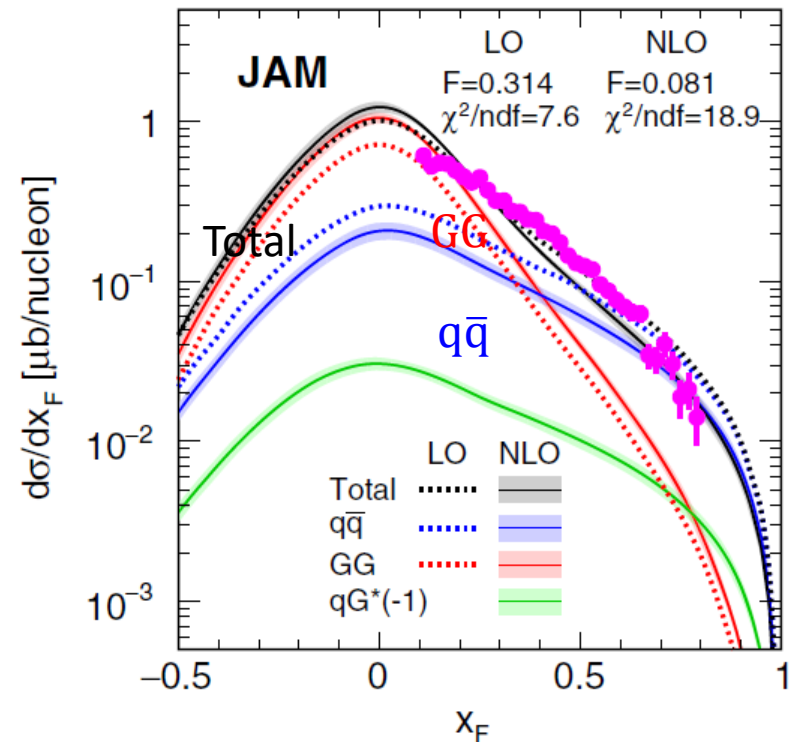hadronization parameter F determined by the fit.

- The GG contribution dominates except at very forward or backward directions.
- The weighting of GG contribution is enhanced in the NLO calculations.

Data vs. CEM LO/NLO

[$\pi^- + Be \rightarrow Jpsi + X$ at 515 GeV, PRD 53, 4723 (1996)]

m_c=1.5 GeV, μ_F=2m_c, μ_R=m_c,
hadronization parameter F determined by the fit.
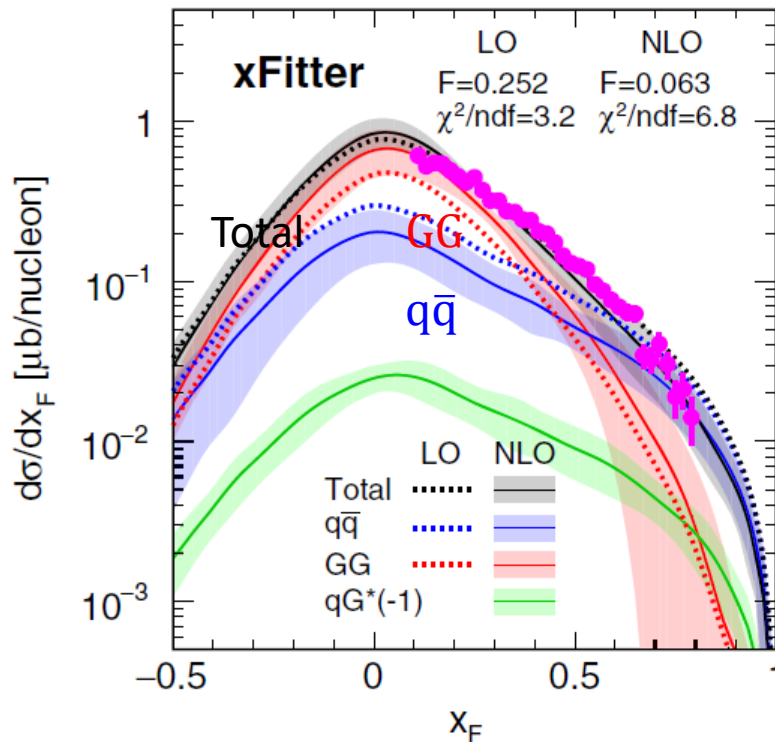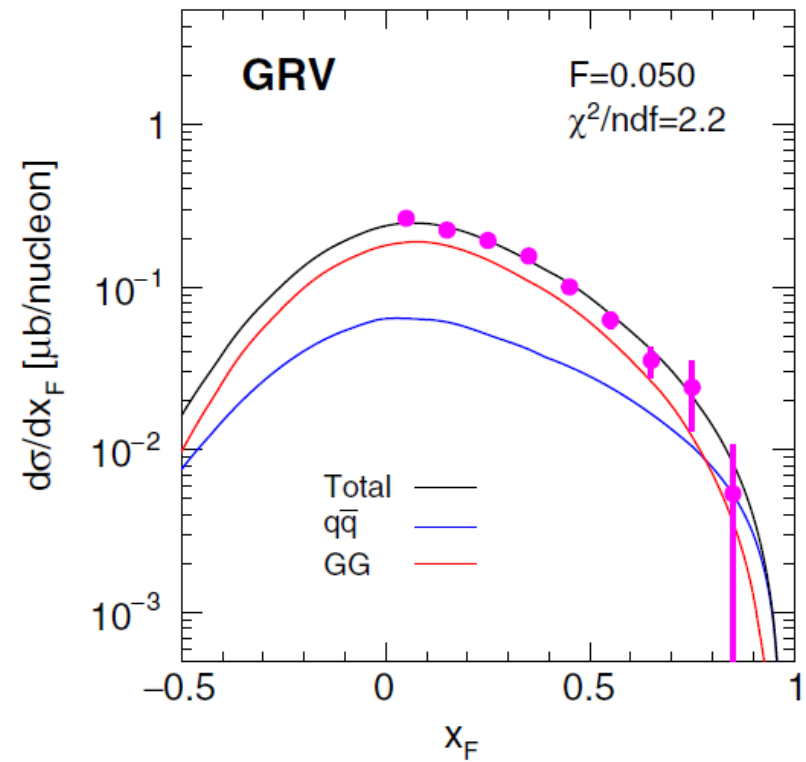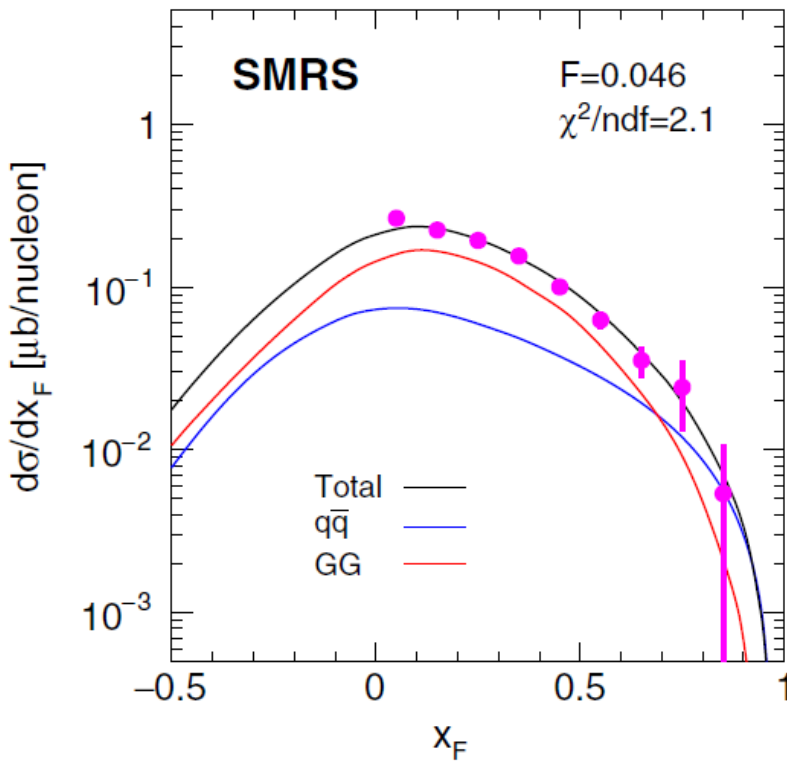

- The GG contribution dominates except at very forward or backward directions.
- The weighting of GG contribution is enhanced in the NLO calculations.

Data vs. CEM NLO

[$\pi^- + Pt \to Jpsi + X$ **at 200 GeV, Z. Phys. C20,101(1983)]**

- To well describe the data for xF>0.2, an appropriate weighting of GG and $q\bar{q}$ contributions is necessary.

Data vs. CEM NLO

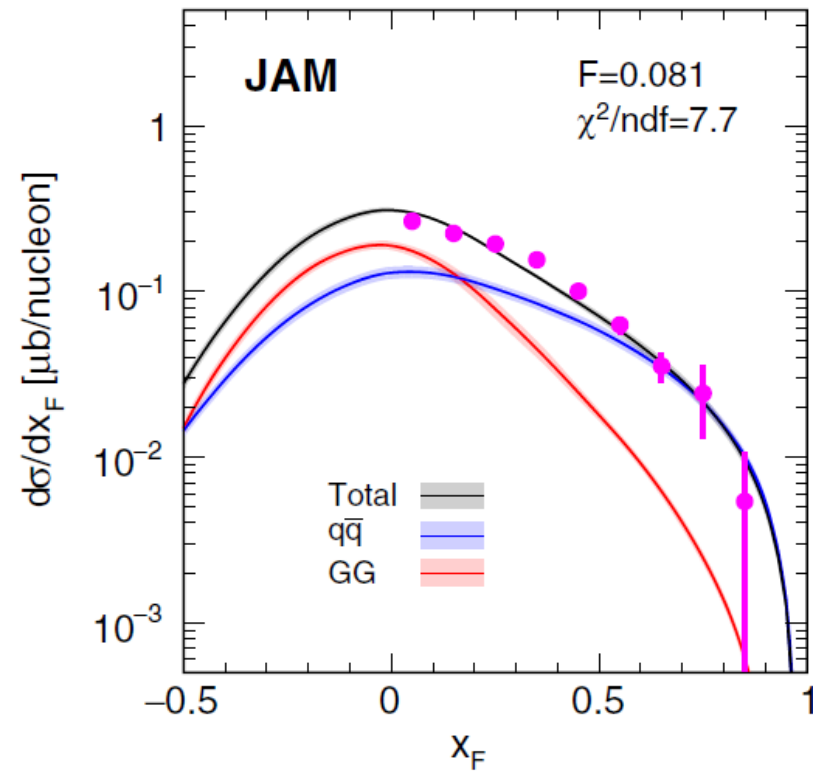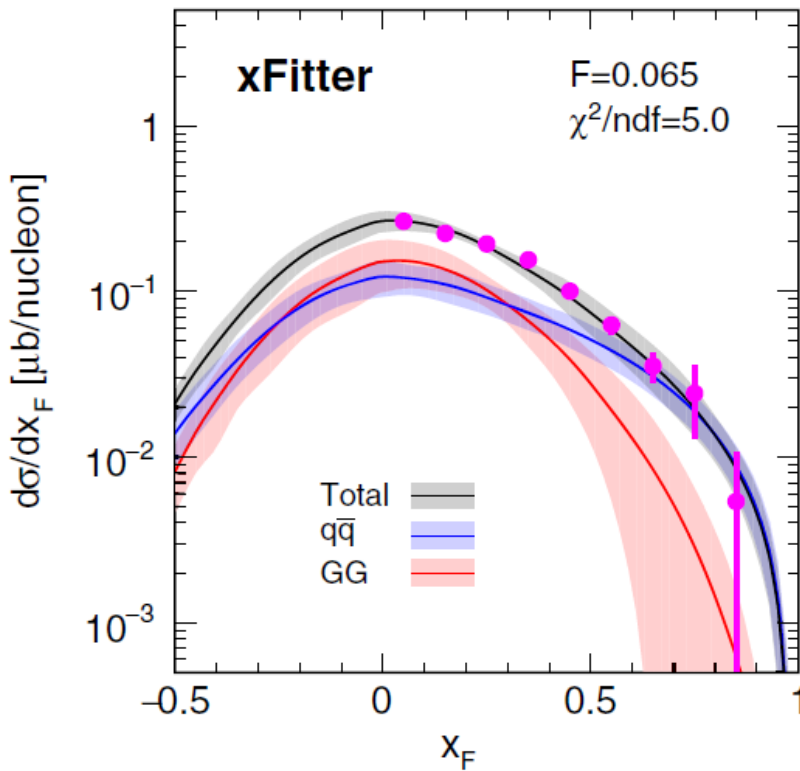[$\pi^- + Pt \to Jpsi + X$ at **200 GeV**, Z. Phys. C20,101(1983)]

- To well describe the data for xF>0.2, an appropriate weighting of GG and q$\bar{q}$ contributions is necessary.

Data vs. CEM NLO

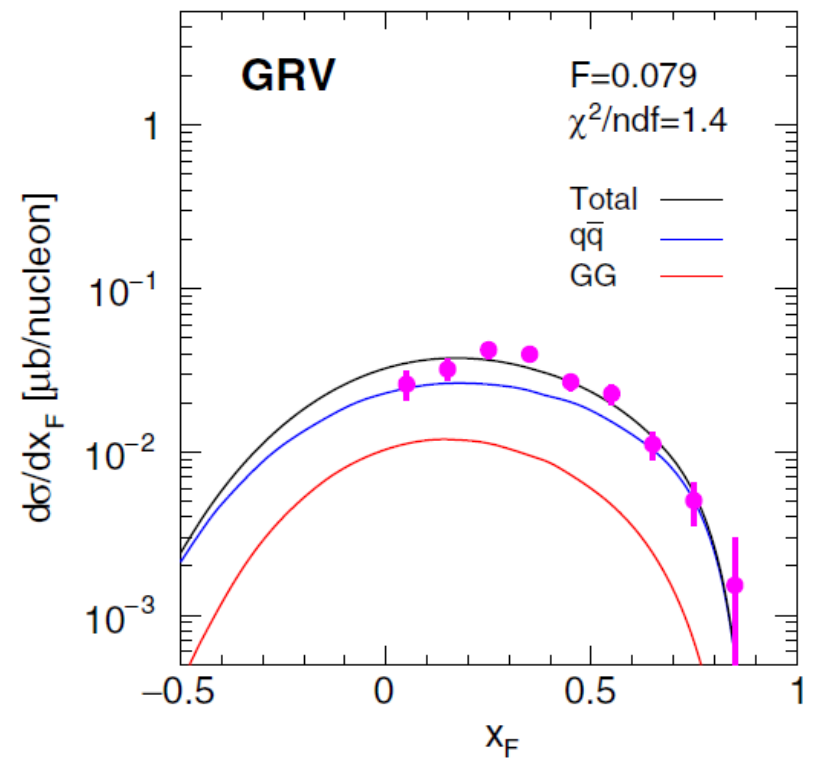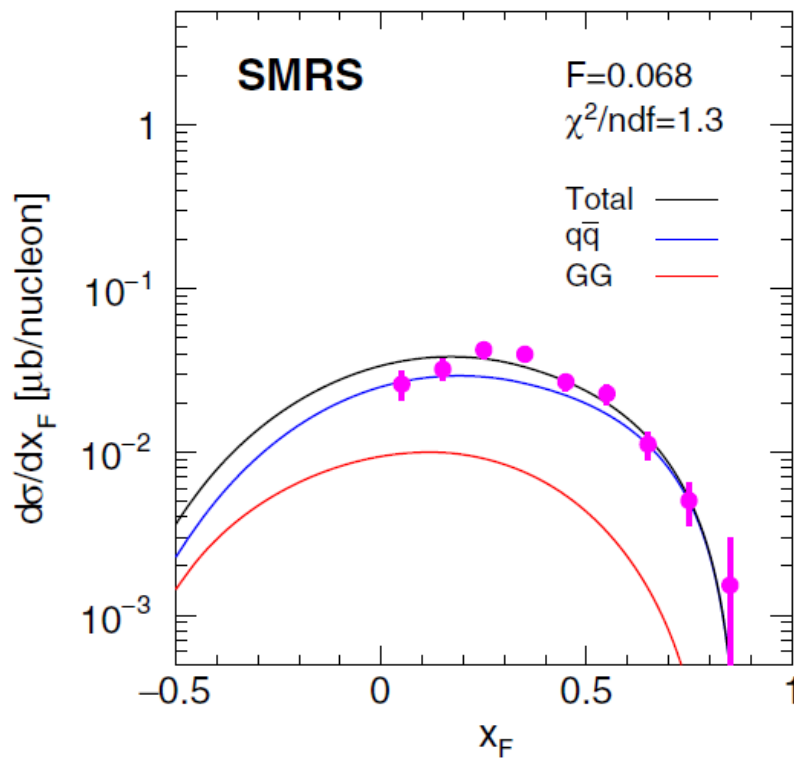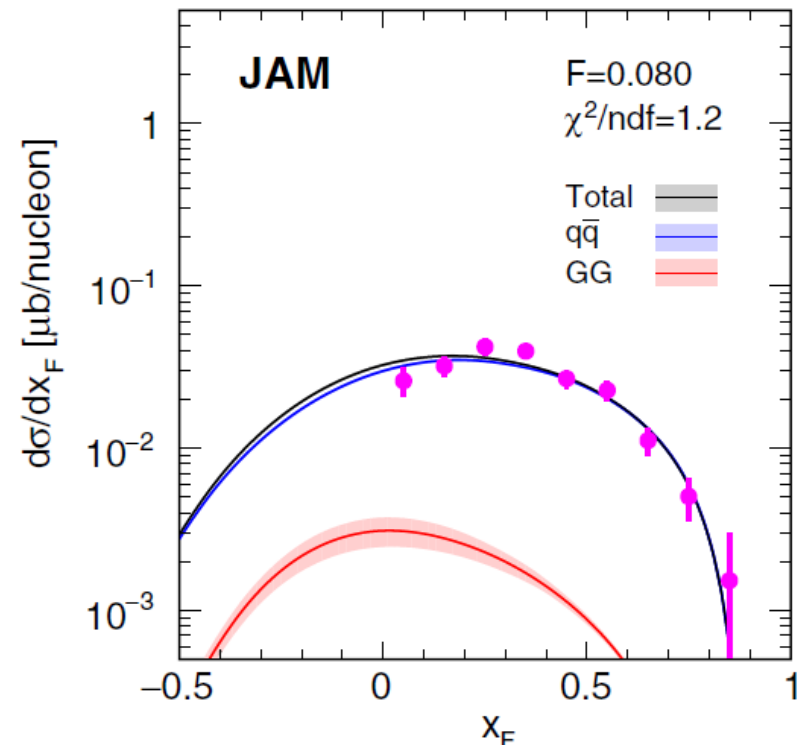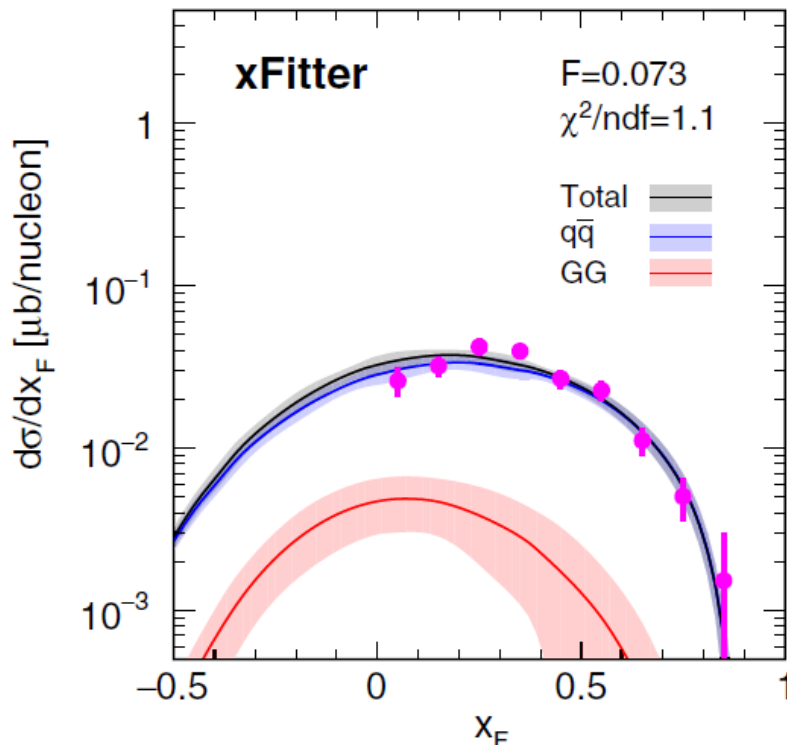[$\pi^- + p \to Jpsi + X$ at **39.5 GeV**, **PLB 98, 220 (1981)**]

- Calculations of all four PDFs describe the data well.

Data vs. CEM NLO

$[\pi^- + p \to Jpsi + X$ at **39.5 GeV**, **PLB 98, 220 (1981)]**

- Calculations of all four PDFs describe the data well.

Data vs. CEM Calculations

TABLE III. Results of F factor and χ^2/ndf value of the best fit of the NLO CEM calculations for SMRS, GRV, xFitter, and JAM pion PDFs to the data listed in Table II. The F^* factor and χ^2/ndf^* are the ones corresponding to the fit with inclusion of PDF uncertainties for xFitter and JAM.

Data	SMRS		GRV		xFitter				JAM			
Experiment (P_{beam})	F	χ^2/ndf	F	χ^2/ndf	F	F^*	χ^2/ndf	χ^2/ndf^*	F	F^*	χ^2/ndf	χ^2/ndf^*
E672, E706 (515)	0.040	1.2	0.040	2.2	0.063	0.063	6.8	4.7	0.081	0.081	18.9	18.5
E705 (300)	0.052	2.3	0.053	1.9	0.073	0.076	3.2	1.3	0.086	0.086	16.1	15.9
NA3 (280)	0.046	1.5	0.049	2.0	0.067	0.069	5.0	3.2	0.081	0.081	10.4	10.3
NA3 (200)	0.046	2.1	0.050	2.2	0.065	0.066	5.0	1.3	0.081	0.081	7.7	7.6
WA11 (190)	0.054	5.0	0.058	7.2	0.078	0.076	19.4	6.2	0.091	0.091	73.7	72.9
NA3 (150)	0.065	1.1	0.071	1.0	0.089	0.091	2.6	1.6	0.108	0.108	3.9	3.8
E537 (125)	0.044	1.5	0.049	1.5	0.065	0.065	3.1	1.4	0.083	0.083	3.5	3.5
WA39 (39.5)	0.068	1.3	0.079	1.4	0.073	0.072	1.1	0.8	0.080	0.080	1.2	1.2

- The hadronization F factor is stable across energy.
- High-energy J/ψ data have a large sensitivity to the large-x gluon density of pions.
- The valence-quark distributions plays a minor role if away from the threshold.
- CEM NLO calculations favor SMRS and GRV PDFs whose gluon densities at x > 0.1 are higher, compared with xFitter and JAM PDFs.
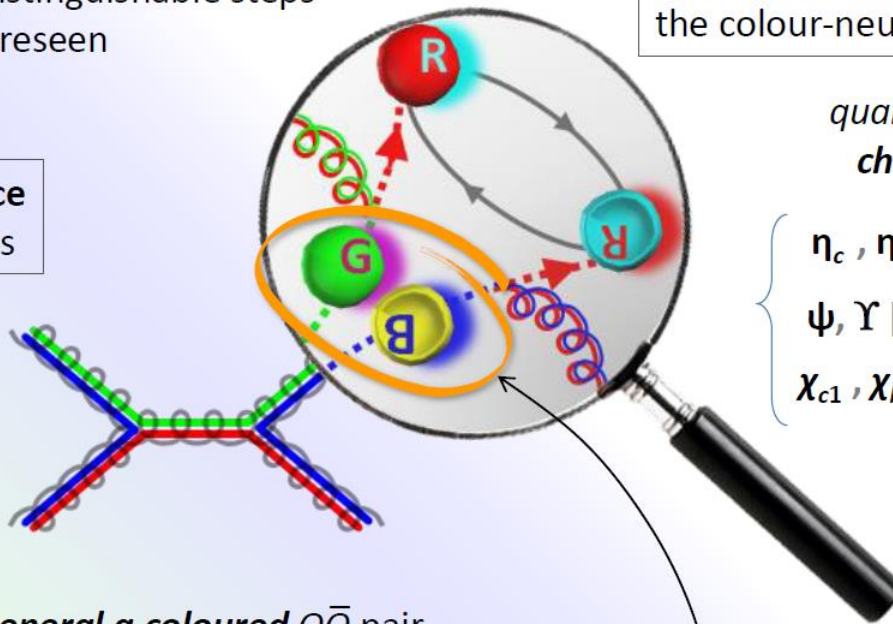
Are these observations model dependent?

33

NRQCD

The "cascade" (*factorization*) approach of NRQCD
Non-Relativistic

For **heavy** quarkonia two distinguishable steps are foreseen

2) **long-distance** evolution to the colour-neutral bound state

quantum numbers change to final

1) **short-distance** partonic process

η_c, η_b [$^1S_0$]

ψ, Υ [$^3S_1$] χ_{c0}, χ_{b0} [$^3P_0$]

χ_{c1}, χ_{b1} [$^3P_1$] χ_{c2}, χ_{b2} [$^3P_2$]

produces *in general a coloured* $Q\bar{Q}$ pair of any $^{2S+1}L_J$ quantum numbers

$^1S_0$ $^1S_0$ $^3S_1$ $^3P_0$ $^3P_2$
$^1D_2$ $^3P_2$ $^3D_3$ $^1P_1$ $^3S_1$
$^3P_1$ $^3P_1$ $^1P_1$
$^3D_2$ $^3D_1$ $^3P_1$

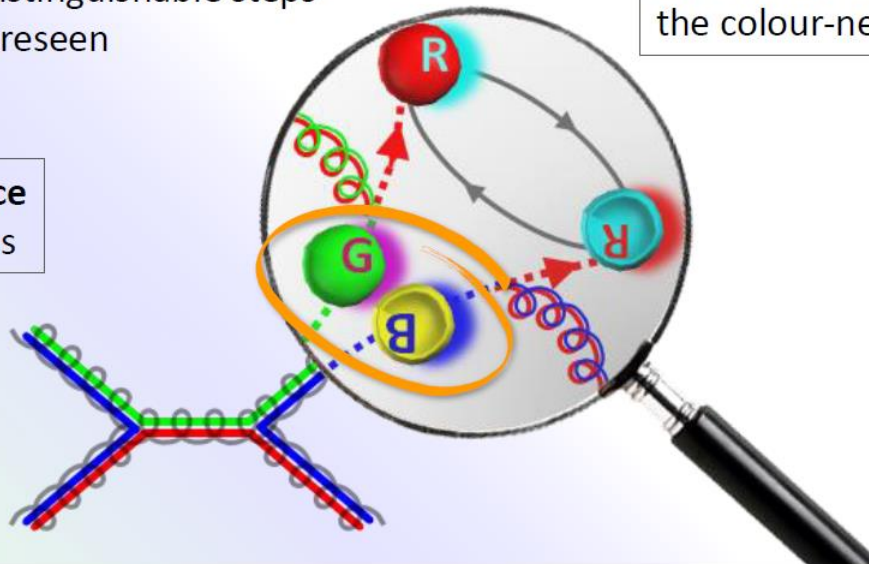Even if the *pre-resonance* $Q\bar{Q}$ state is not observed, it determines, with its own quantum properties, the observable kinematics and *polarization*

34

NRQCD

The "cascade" (*factorization*) approach of NRQCD

For **heavy** quarkonia two distinguishable steps are foreseen

2) **long-distance** evolution to the colour-neutral bound state

1) **short-distance** partonic process

1) *short-distance coefficients* (**SDCs**): p_T-dependent partonic cross sections

2) *long-distance matrix elements* (**LDMEs**): constant, **fitted from data**

$$\sigma(A + B \to \mathcal{Q} + X) = \sum_{S, L, C} \mathcal{S}\{A + B \to (Q\bar{Q})_C[^{2S+1}L_J] + X\} \cdot \mathcal{L}\{(Q\bar{Q})_C[^{2S+1}L_J] \to \mathcal{Q}\}$$

$Q\bar{Q}$ **angular momentum** and **colour** configurations

35

Beneke and Krämer
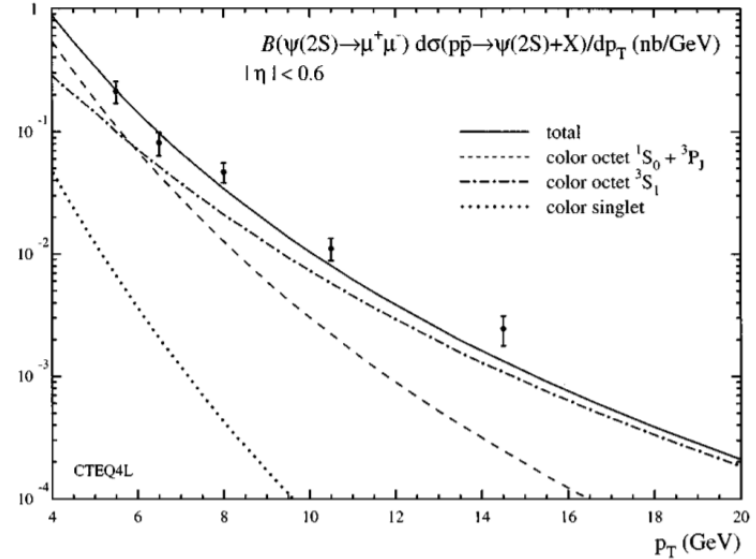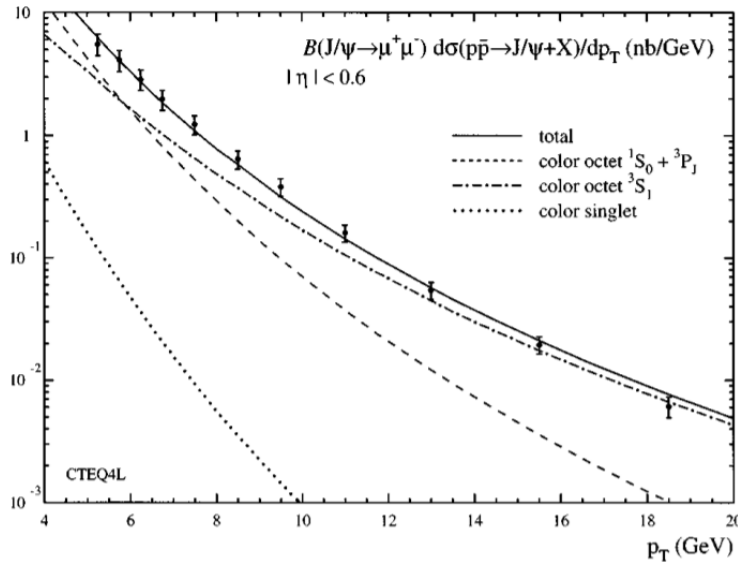## PRD 55, R5269(R) (1997)

Color octet >> color singlet

$B(J/\psi \to \mu^+\mu^-) \, d\sigma(p\bar{p} \to J/\psi + X)/dp_T$ (nb/GeV)

$|\eta| < 0.6$

- total
- color octet $^1S_0 + {}^3P_J$
- color octet $^3S_1$
- color singlet

CTEQ4L

p_T (GeV)

$B(\psi(2S) \to \mu^+\mu^-) \, d\sigma(p\bar{p} \to \psi(2S) + X)/dp_T$ (nb/GeV)

$|\eta| < 0.6$

- total
- color octet $^1S_0 + {}^3P_J$
- color octet $^3S_1$
- color singlet

CTEQ4L

p_T (GeV)

TABLE I. NRQCD matrix elements in 10^{-2} GeV^3. First error statistical, second error due to variation of scale. Ratio of ψ' to J/ψ fixed.

	CTEQ4L	GRV (1994) LO	MRS(R2)
$\langle \mathcal{O}_8^{J/\psi}(^3S_1) \rangle$	$1.06 \pm 0.14^{+1.05}_{-0.59}$	$1.12 \pm 0.14^{+0.99}_{-0.56}$	$1.40 \pm 0.22^{+1.35}_{-0.79}$
$M_{3.5}^{J/\psi}(^1S_0^{(8)}, {}^3P_0^{(8)})$	$4.38 \pm 1.15^{+1.52}_{-0.74}$	$3.90 \pm 1.14^{+1.46}_{-1.07}$	$10.9 \pm 2.07^{+2.79}_{-1.26}$
$\langle \mathcal{O}_8^{\psi'}(^3S_1) \rangle$	$0.44 \pm 0.08^{+0.43}_{-0.24}$	$0.46 \pm 0.08^{+0.41}_{-0.23}$	$0.56 \pm 0.11^{+0.54}_{-0.32}$
$M_{3.5}^{\psi'}(^1S_0^{(8)}, {}^3P_0^{(8)})$	$1.80 \pm 0.56^{+0.62}_{-0.30}$	$1.60 \pm 0.51^{+0.60}_{-0.44}$	$4.36 \pm 0.96^{+1.11}_{-0.50}$

36

NRQCD: partial NLO
PRD 54 (1996) 2005

Hadroproduction of quarkonium in fixed-target experiments

M. Beneke
Stanford Linear Accelerator Center, Stanford University, Stanford, California 94309

I. Z. Rothstein
University of California, San Diego, 9500 Gilman Drive, La Jolla, California 92093
(Received 25 March 1996)

We analyze charmonium and bottomonium production at fixed-target experiments. We find that the inclusion of color octet production channels removes large discrepancies between experiment and the predictions of the color singlet model for the total production cross section. Furthermore, including octet contributions accounts for the observed direct to total J/ψ production ratio. As found earlier for photoproduction of quarkonia, a fit to fixed-target data requires smaller color octet matrix elements than those extracted from high-p_t production at the Fermilab Tevatron. We argue that this difference can be explained by systematic differences in the velocity expansion for collider and fixed-target predictions. While the color octet mechanism thus appears to be an essential part of a satisfactory description of fixed-target data, important discrepancies remain for the χ_{c1}/χ_{c2} production ratio and J/ψ (ψ') polarization. These discrepancies, as well as the differences between pion- and proton-induced collisions, emphasize the need for including higher twist effects in addition to the color octet mechanism. [S0556-2821(96)05515-4]
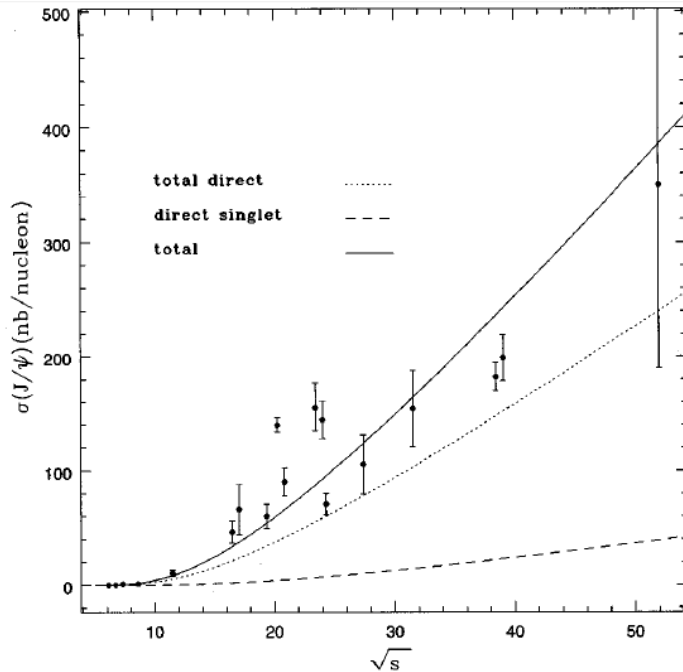
Beneke & Roshstein,
PRD 54 (1996) 2005

FIG. 2. J/ψ production cross sections in proton-nucleon collisions for $x_F > 0$. The dotted line is the direct J/ψ production rate in the CSM and the dashed line includes the contribution from the color octet processes. The total cross section (solid line) includes radiative feeddown from the χ_{cJ} and ψ' states. The solid line is obtained with $\Delta_8(J/\psi) = 3.0 \times 10^{-2}$ GeV^3.
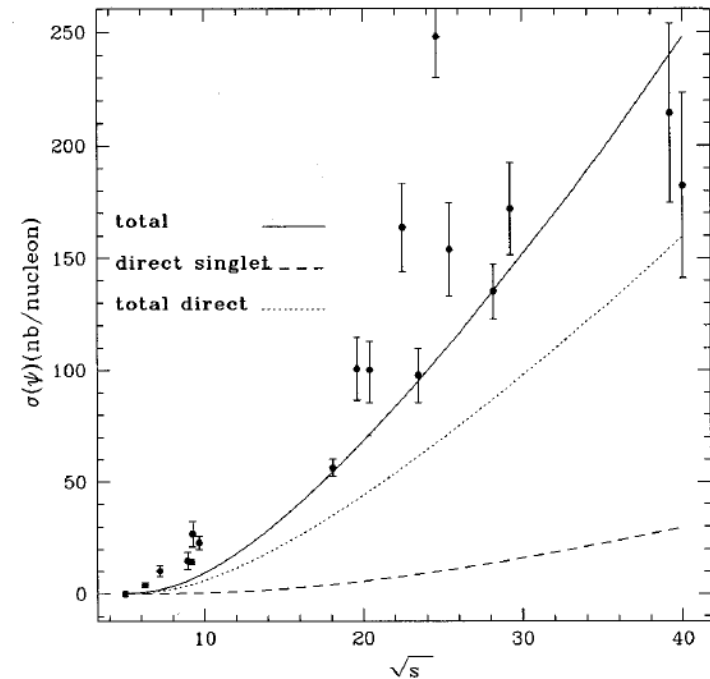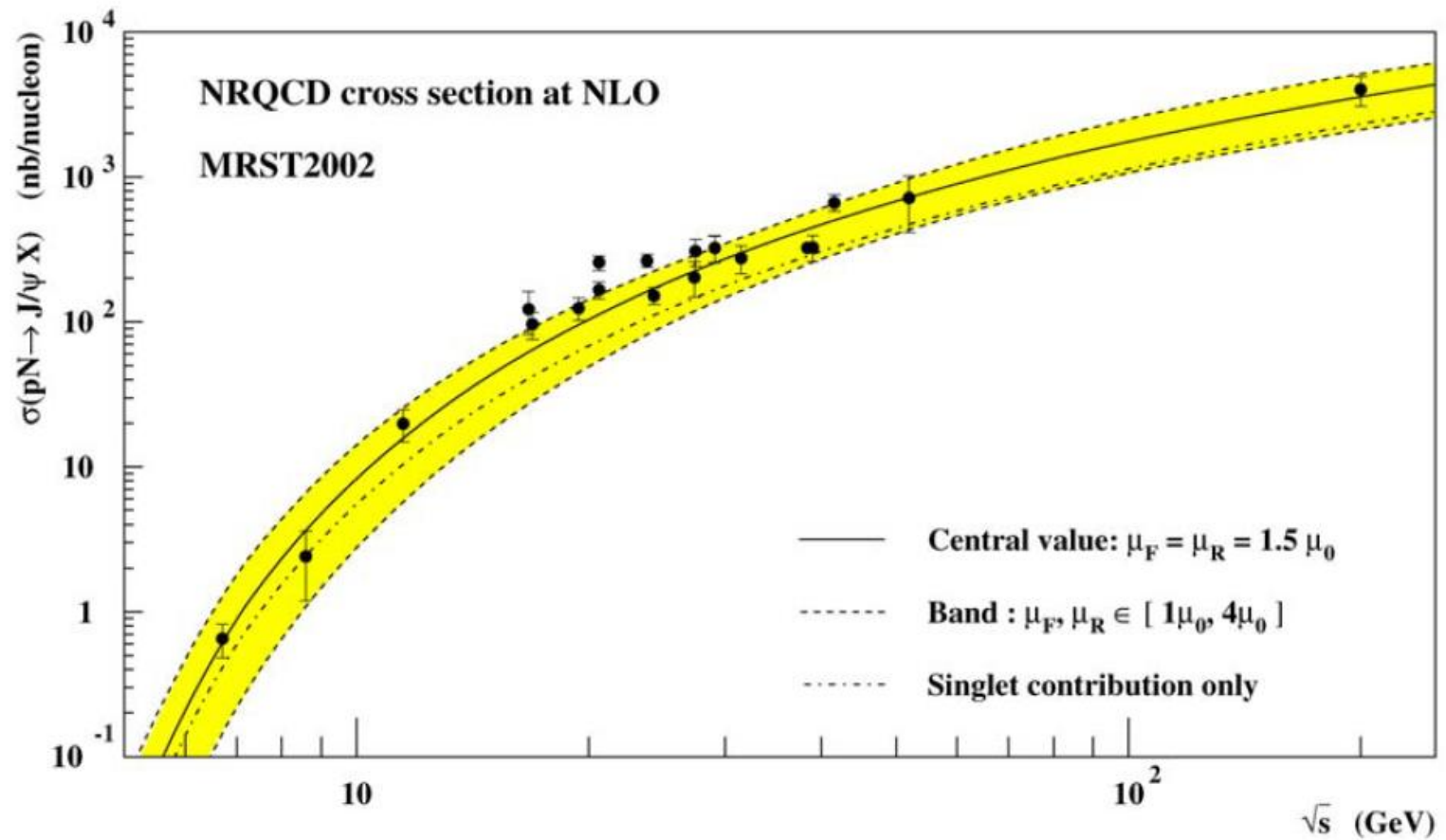
FIG. 5. J/ψ production cross sections in pion-nucleon collisions for $x_F > 0$. Direct J/ψ production in the CSM (dashed line) and after inclusion of color octet processes (dotted line). The total cross section (solid line) includes radiative feeddown from the χ_{cJ} and ψ' states. The solid line is obtained with $\Delta_8(J/\psi) = 3.0 \times 10^{-2}$ GeV^3.

Direct/octet contribution dominates (75-80%)!

38

Maltoni, et al.,
PLB 638 (2006) 202

Long-Distance Matrix Elements

LDME1

LDME2

H	$\langle \mathcal{O}_1^H \rangle$	$\langle \mathcal{O}_8^H[^3S_1] \rangle$	$\langle \mathcal{O}_8^H[^1S_0] \rangle = \langle \mathcal{O}_8^H[^3P_0]/m_c^2 \rangle$
J/ψ	$1.16\,\text{GeV}^3$	$0.66\text{x}10^{-2}\,\text{GeV}^3$	$0.375\text{x}10^{-2}\,\text{GeV}^3$
$\Psi(2S)$	$0.76\,\text{GeV}^3$	$0.46\text{x}10^{-2}\,\text{GeV}^3$	$0.065\text{x}10^{-2}\,\text{GeV}^3$
ξ_{c0}	$0.044\,\text{GeV}^3$	$0.32\text{x}10^{-2}\,\text{GeV}^3$	

Beneke, Routhstein
PRD 54, 2005 (1996)

H	$\langle \mathcal{O}_1^H \rangle$	$\langle \mathcal{O}_8^H[^3S_1] \rangle$	$\langle \mathcal{O}_8^H[^1S_0] \rangle = \langle \mathcal{O}_8^H[^3P_0]/m_c^2 \rangle$
J/ψ	$1.16\,\text{GeV}^3$	$1.19\text{x}10^{-2}\,\text{GeV}^3$	$1.0\text{x}10^{-2}\,\text{GeV}^3$
$\Psi(2S)$	$0.76\,\text{GeV}^3$	$0.5\text{x}10^{-2}\,\text{GeV}^3$	$0.42\text{x}10^{-2}\,\text{GeV}^3$
ξ_{c0}	$0.11\,\text{GeV}^3$	$0.31\text{x}10^{-2}\,\text{GeV}^3$	

Maltoni et al.,
PLB638, 202 (2006)

TABLE I. Two sets of NRQCD matrix elements for charmonium production

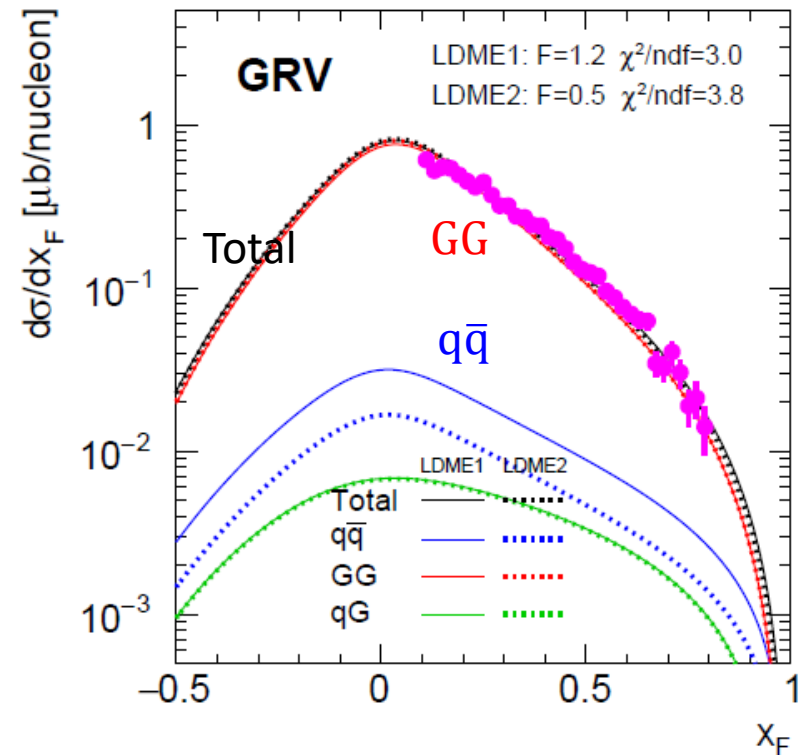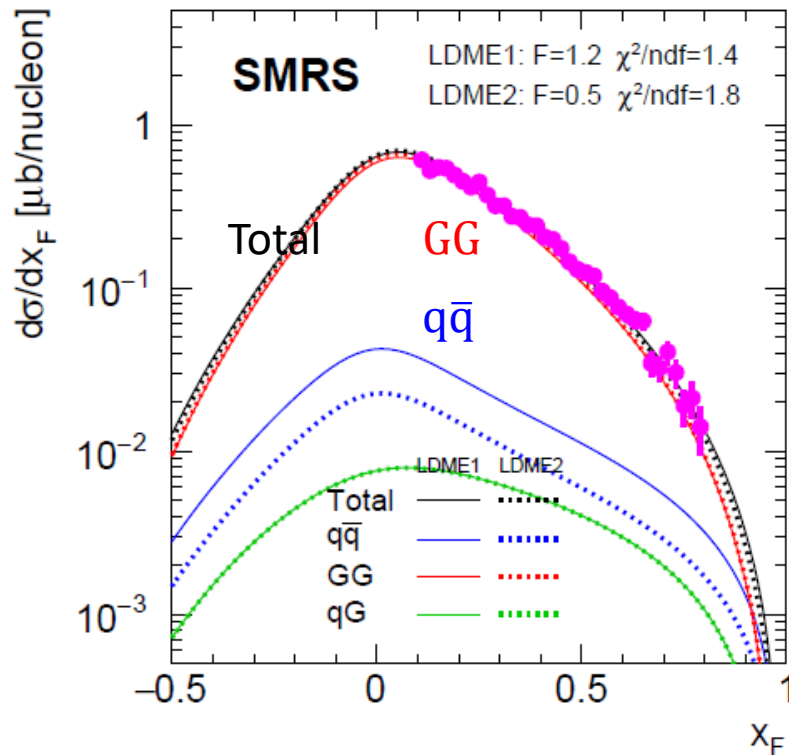# Data vs. NRQCD
: Energy dependence

LDME1

LDME2
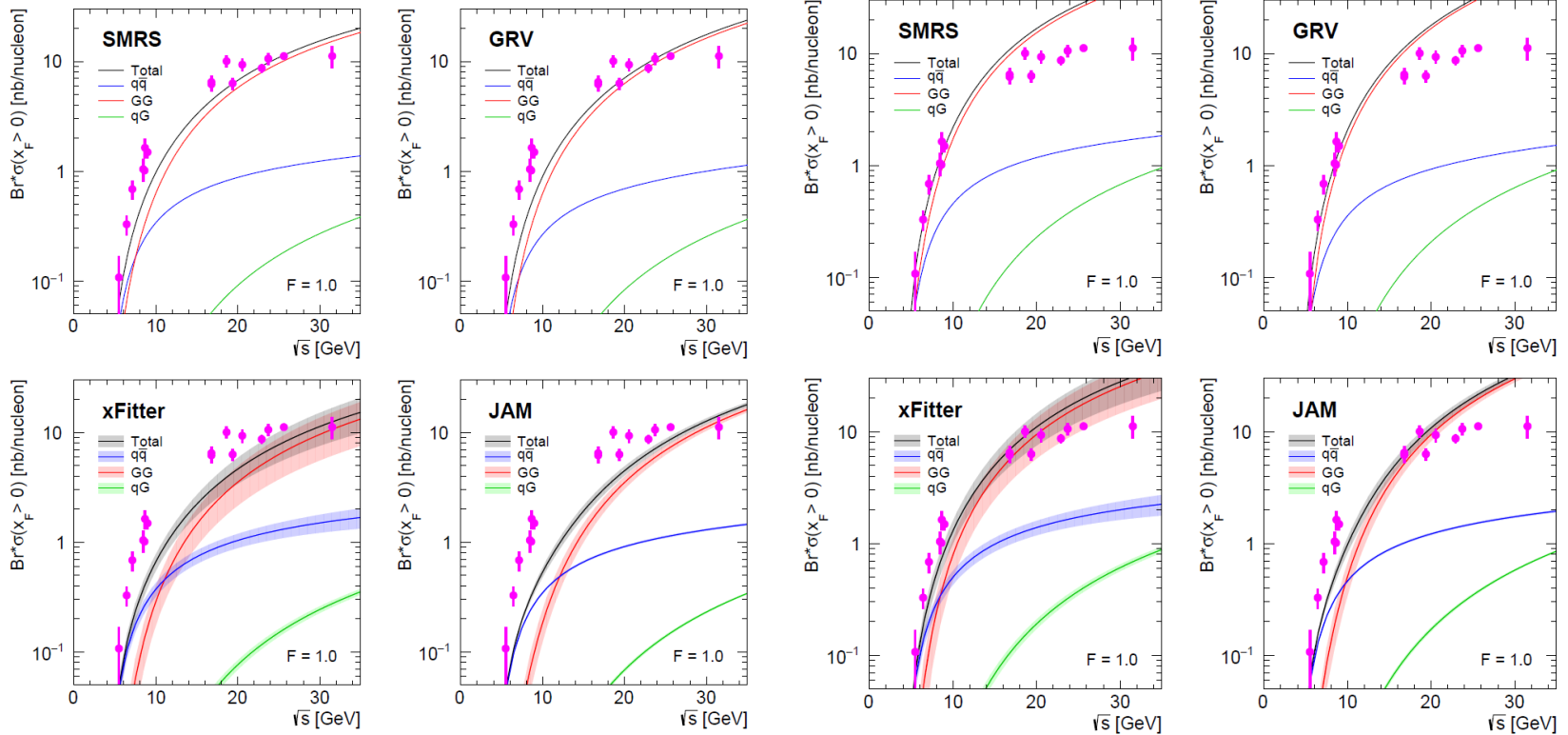
GG dominates at high energies while qqbar is important near threshold.

Data vs. NRQCD

[$\pi^- + Be \rightarrow Jpsi + X$ at 515 GeV, PRD 53, 4723 (1996)]

m_c=1.5 GeV, μ_F=2m_c, μ_R=2m_c,
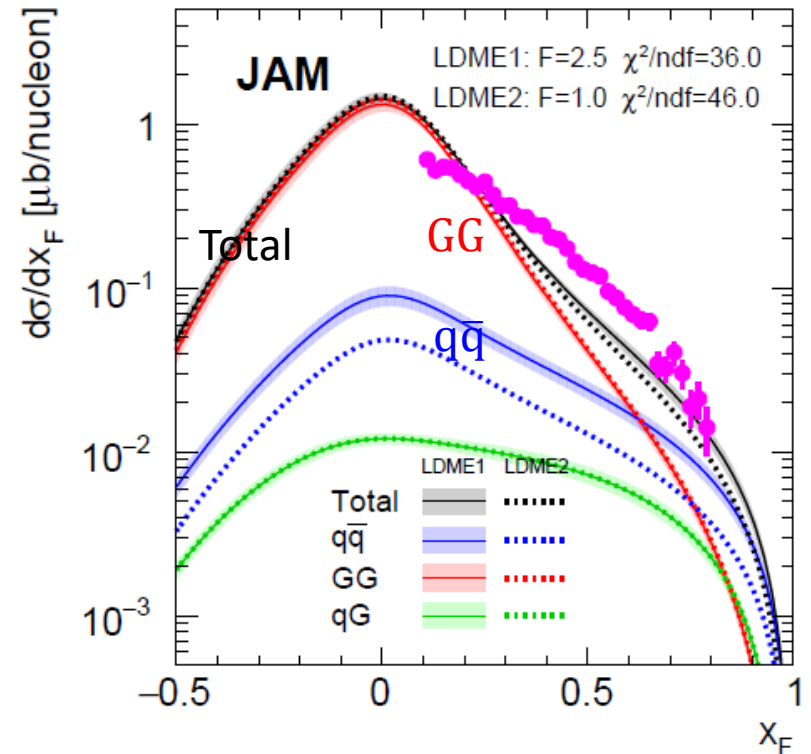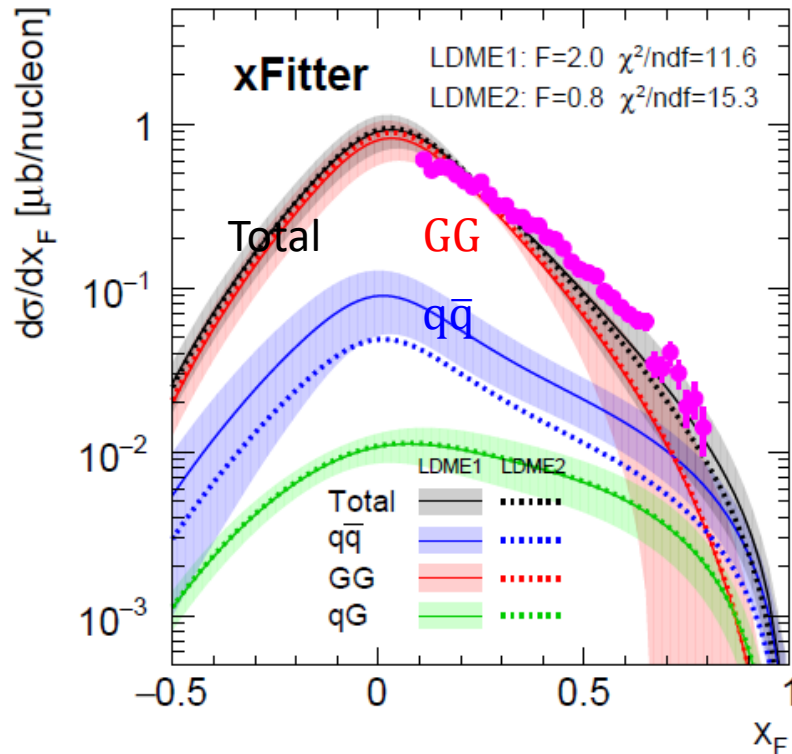Normalization parameter F determined by the fit.

- The GG contribution dominates except at very forward or backward directions.

Data vs. NRQCD

[$\pi^- + Be \to Jpsi + X$ at **515** GeV, PRD 53, 4723 (1996)]
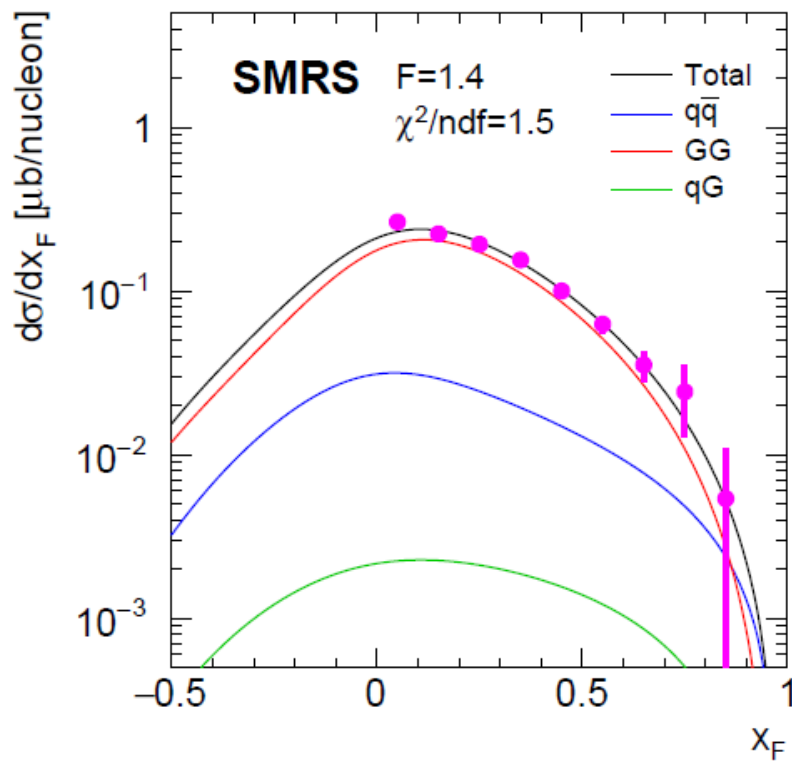
m_c=1.5 GeV, μ_F=2m_c, μ_R=2m_c,
Normalization parameter F determined by the fit.

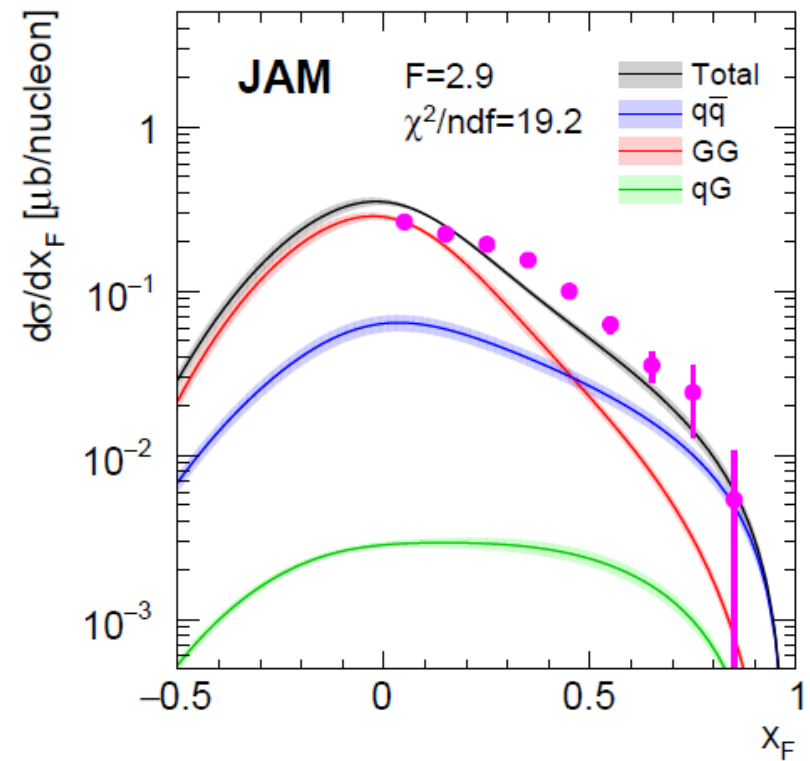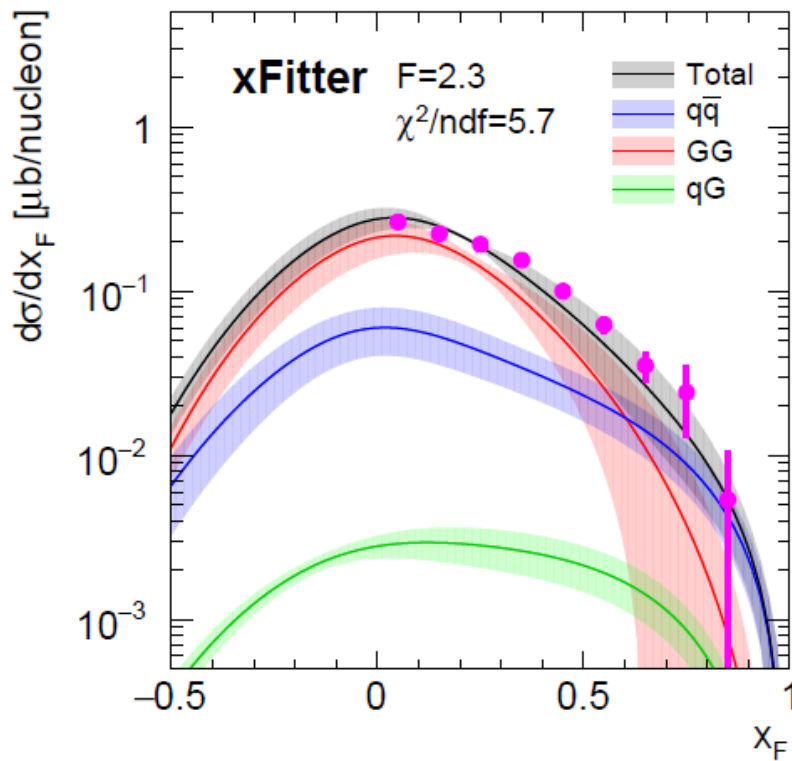- The GG contribution dominates except at very forward or backward directions.

Data vs. NRQCD

[$\pi^- + Pt \rightarrow Jpsi + X$ at 200 GeV, Z. Phys. C20,101(1983)]
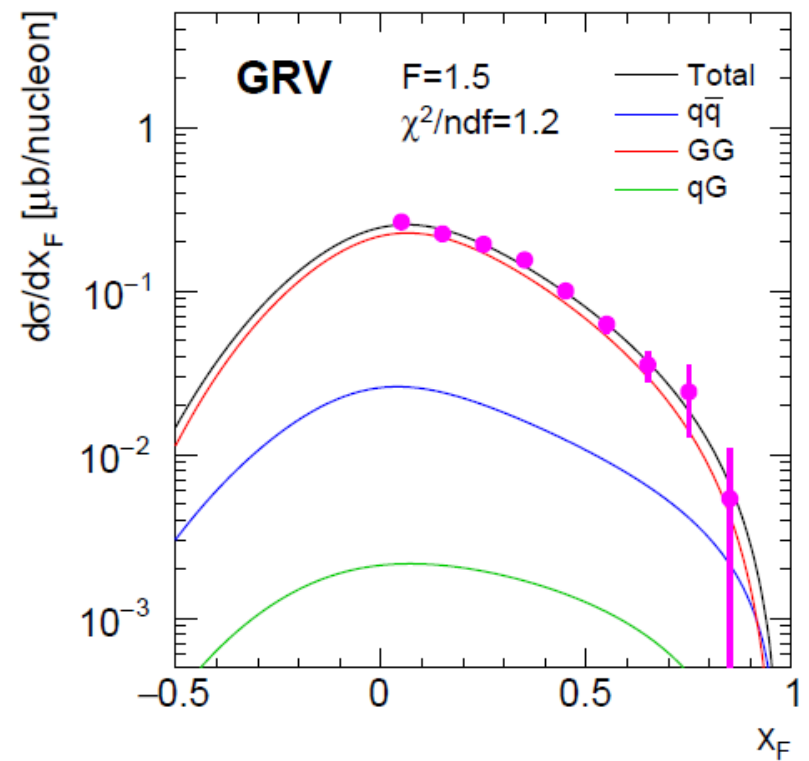
• To well describe the data for xF>0.2, an appropriate weighting of GG and q$\bar{q}$ contributions is necessary.

Data vs. NRQCD
[$\pi^- + Pt \rightarrow Jpsi + X$ at 200 GeV, Z. Phys. C20,101(1983)]

- To well describe the data for xF>0.2, an appropriate weighting of GG and q$\bar{q}$ contributions is necessary.
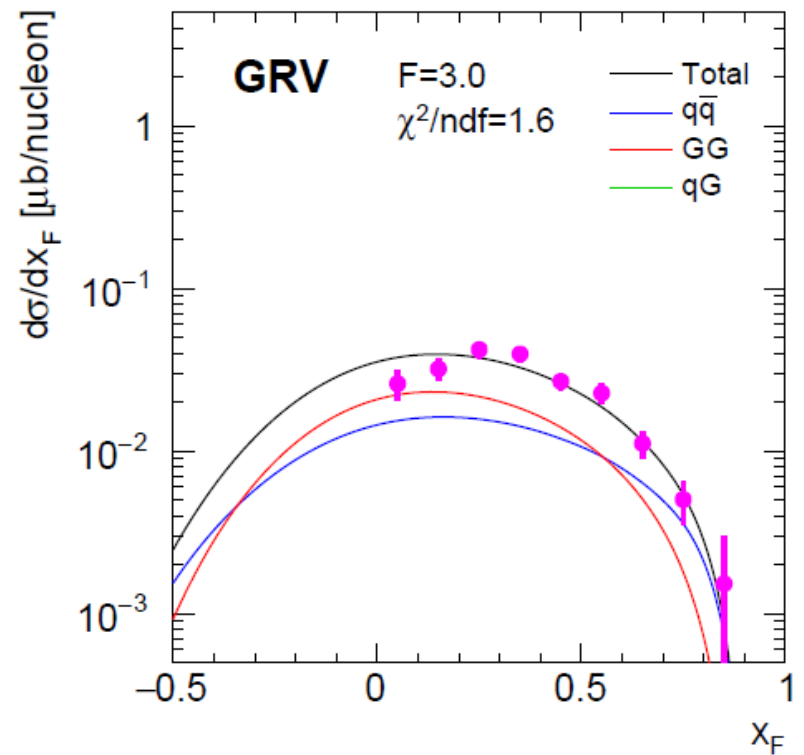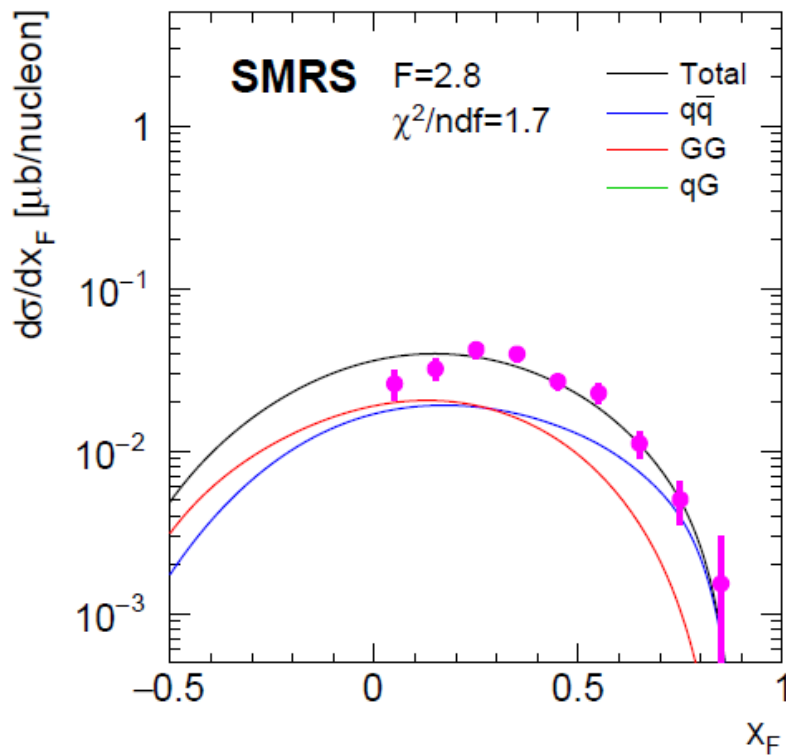
45

Data vs. NRQCD

$[\pi^- + p \rightarrow Jpsi + X$ **at** 39.5 **GeV, PLB 98, 220 (1981)]**

- Calculations of all four PDFs describe the data well.

Data vs. NRQCD
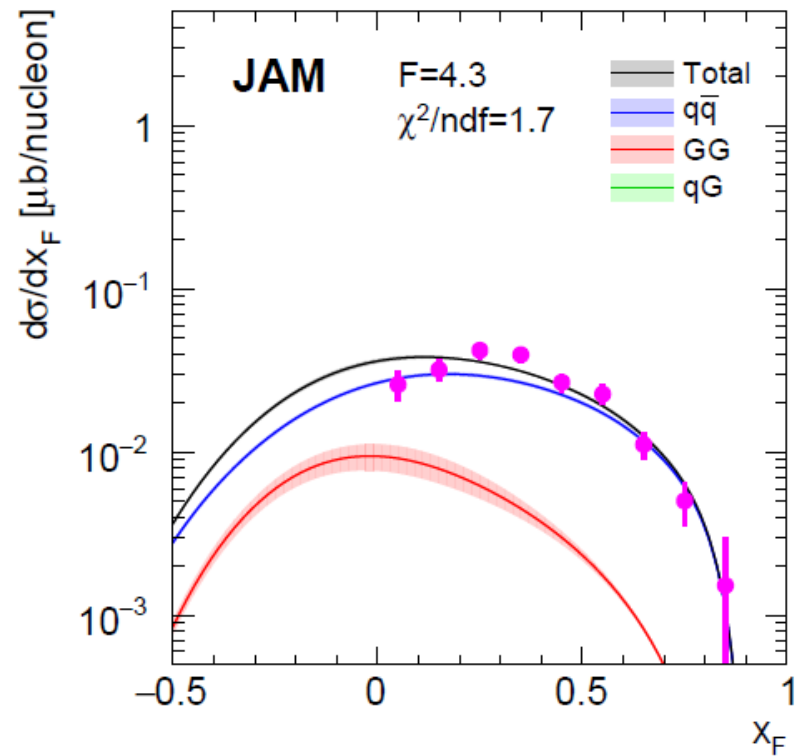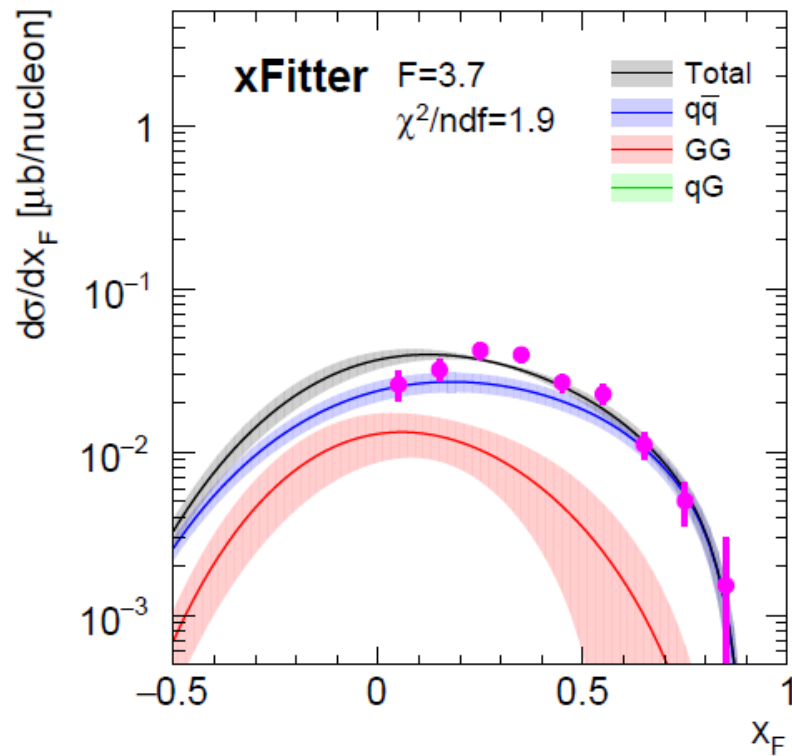
$[\pi^- + p \rightarrow Jpsi + X$ **at** 39.5 **GeV, PLB 98, 220 (1981)]**

- Calculations of all four PDFs describe the data well.

Data vs. NRQCD

[$\pi^- + Be \to Jpsi + X$ at 515 GeV, PRD 53, 4723 (1996)]

m_c=1.5 GeV, μ_F=2m_c, μ_R=2m_c,
Normalization parameter F determined by the fit.
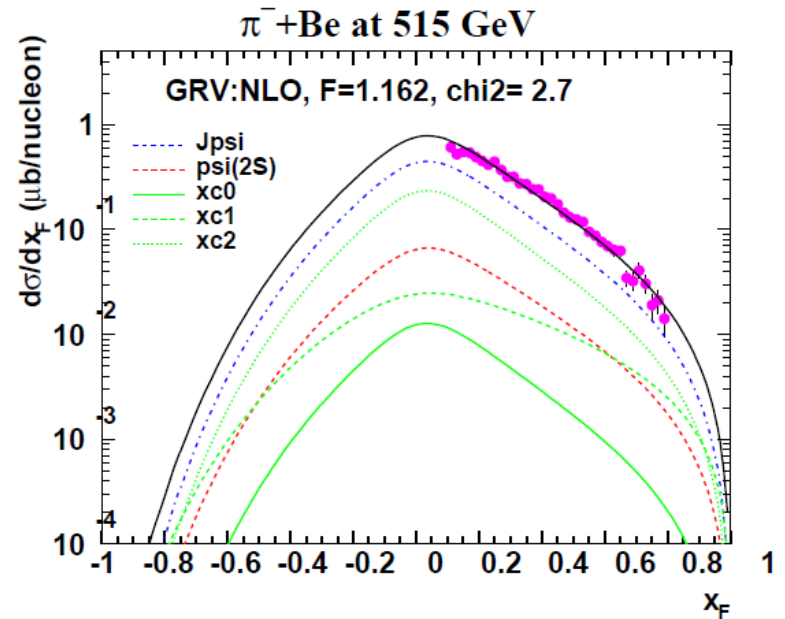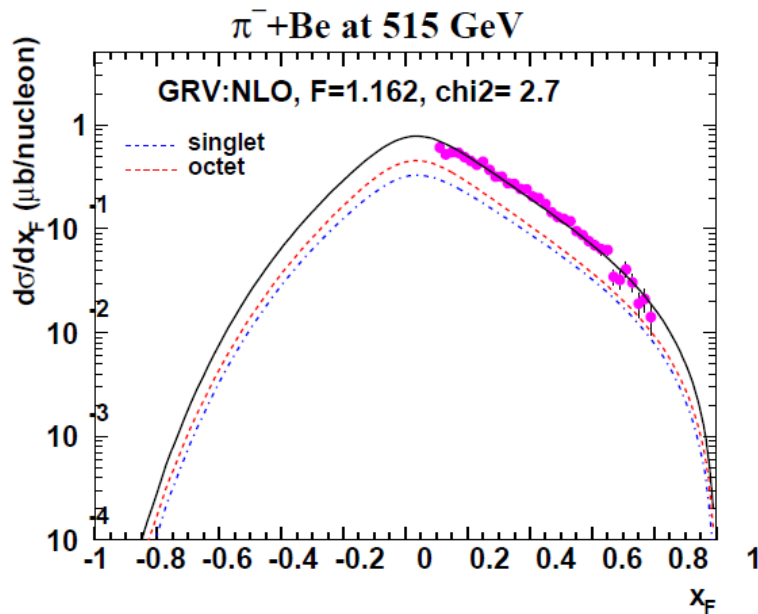
Data vs. NRQCD
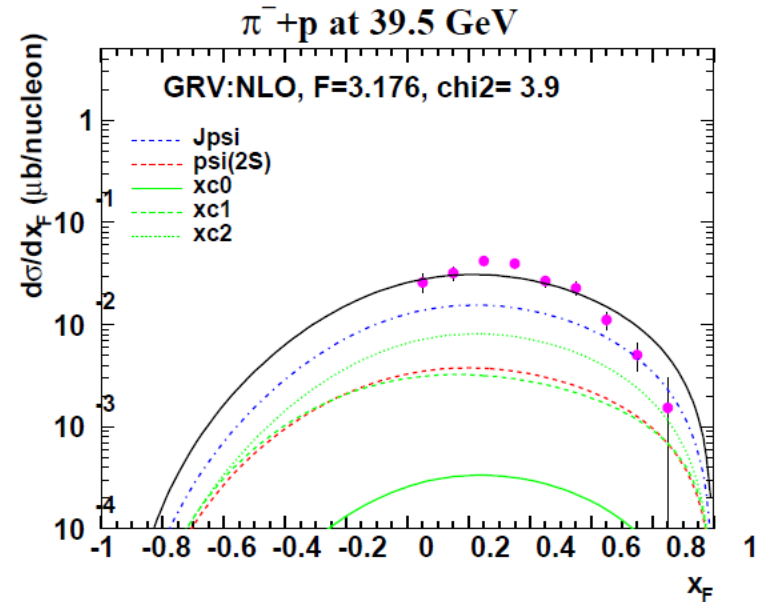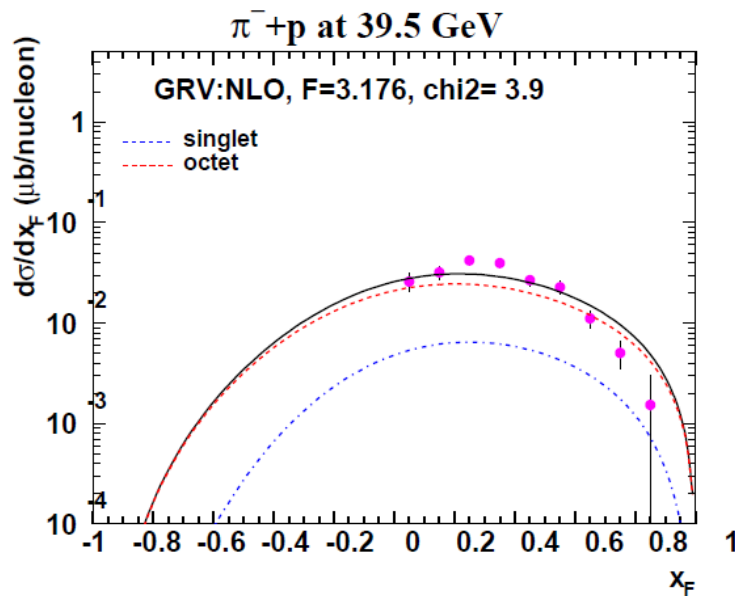[$\pi^- + p \rightarrow Jpsi + X$ at 39.5 GeV, PLB 98, 220 (1981)]

m_c=1.5 GeV, μ_F=2m_c, μ_R=2m_c,
Normalization parameter F determined by the fit.

LDME1

LDME2

Data	SMRS		GRV		xFitter				JAM			
Experiment (P_{beam})	F	χ^2/ndf	F	χ^2/ndf	F	F^*	χ^2/ndf	χ^2/ndf*	F	F^*	χ^2/ndf	χ^2/ndf*
E672, E706 (515)	1.194	1.4	1.171	3.0	1.977	1.985	11.6	10.7	2.524	2.603	36.0	29.5
E705 (300)	1.504	2.7	1.477	2.5	2.270	2.261	5.2	4.4	2.555	2.564	29.8	20.1
NA3 (280)	1.332	2.5	1.374	3.2	2.152	2.154	9.6	8.6	2.449	2.620	24.4	17.3
NA3 (200)	1.387	1.5	1.460	1.2	2.274	2.276	5.7	3.9	2.866	3.226	19.2	6.7
WA11 (190)	1.609	3.2	1.643	7.8	2.541	2.529	27.1	20.0	2.816	2.793	137.5	69.4
NA3 (150)	2.040	2.2	2.141	2.2	3.283	3.314	6.9	6.0	4.081	4.595	12.9	7.1
E537 (125)	1.324	2.7	1.451	2.0	2.277	2.263	6.9	5.5	3.113	3.422	13.2	5.0
WA39 (39.5)	2.785	1.7	3.019	1.6	3.656	3.688	1.9	1.7	4.337	4.456	1.7	1.1
E672, E706 (515)	0.476	1.8	0.462	3.8	0.802	0.805	15.3	14.2	1.013	1.049	46.0	38.1
E705 (300)	0.592	2.8	0.573	2.7	0.916	0.912	6.0	5.1	1.017	1.020	35.6	24.0
NA3 (280)	0.529	3.0	0.540	3.9	0.884	0.883	12.1	10.8	0.983	1.060	30.9	22.4
NA3 (200)	0.556	1.5	0.579	1.1	0.962	0.958	6.9	5.5	1.215	1.408	26.8	10.1
WA11 (190)	0.642	3.0	0.645	7.7	1.056	1.047	31.4	23.0	1.142	1.131	169.5	84.2
NA3 (150)	0.832	2.8	0.859	2.7	1.424	1.438	9.9	8.7	1.779	2.065	19.4	11.6
E537 (125)	0.534	3.2	0.577	2.3	0.981	0.973	9.1	7.2	1.382	1.564	19.8	7.7
WA39 (39.5)	1.386	2.1	1.425	1.9	2.153	2.162	2.8	2.4	2.801	2.904	2.1	1.2

TABLE IV. Results of F factor and χ^2/ndf value of the best fit of the NRQCD calculations with two sets of LDMEs for SMRS, GRV, xFitter, and JAM pion PDFs to the data listed in Table III. The F^* factor and χ^2/ndf* are the ones corresponding to the fit with inclusion of PDF uncertainties for xFitter and JAM.

Summary

- Pion PDFs have been determined by the Drell-Yan, direct photon, J/psi and recently leading-neutron data. Nevertheless discrepancy of valence quark and gluon densities at x>0.1 is seen.

- Within CEM, the high-energy large-x_F J/psi data are shown to be sensitive to the pion gluon distribution at x>0.1. **The current data favor the SMRS and GRV pion PDFs, containing relatively larger gluon content at large x.**

- The same conclusions about pion PDFs are also supported in a similar study in the context of NRQCD.